広島大学学位請求論文

Numerical Simulations of Bifurcation Phenomena in Reaction Diffusion Systems

反応拡散系における分岐現象の数値シミュレーション

2010 年

広島大学理学研究科
数理分子生命理学専攻

高石 武史
(広島国際学院大学 情報デザイン学部)

目次

1. 主論文

Numerical Simulations of Bifurcation Phenomena in Reaction Diffusion Systems
反応拡散系における分岐現象の数値シミュレーション
高石 武史

2. 公表論文

(1) Phase Field Model for Mode III Crack Growth in Two Dimensional Elasticity
T.Takaishi and M.Kimura
Kybernetika 45(4) (2009), 605-614.

(2) Pattern Formation in Coupled Reaction-Diffusion System
T.Takaishi, M.Mimura and Y.Nishiura
Japan Journal of Industrial and Applied Mathematics 12(3) (1995) 385-424.

3. 参考論文

(1) モードIII 亀裂進展のフェーズフィールドモデルとその数値計算
高石 武史
日本応用数理学会論文誌 19(3) (2009), 351-369.

(2) Quantitative study of adaptive mesh FEM with localization index of pattern
M.Kimura, H. Komura, M. Mimura, H. Miyoshi, T. Takaishi, and D. Ueyama
in: Proc. of the Czech-Japanese Seminar in Applied Mathematics 2006,
COE Lecture Note Vol.6, Faculty of Mathematics, Kyushu University
ISSN 1881-4042(2007), 114-136.

(3) Adaptive mesh finite element method for pattern dynamics in reaction-diffusion systems
M. Kimura, H. Komura, M. Mimura, H. Miyoshi, T. Takaishi, and D. Ueyama
in: Proc. of the Czech-Japanese Seminar in Applied Mathematics 2005,
COE Lecture Note Vol.3, Faculty of Mathematics, Kyushu University
ISSN 1881-4042(2006), 56-68.

(4) Charge Variation Effects on Low-Frequency Electrostatic Waves in Dusty Plasmas
T. Takaishi, M. Yabuhara, and K. Nishikawa
Journal of Physical Society Japan, 70 (2001), No.1, 138-143.

(5) Stability Analysis of Wave Propagation in 2-fluid Dusty Plasma System
T. Takaishi and K. Kusano
Journal of Plasma and Fusion Research Series, 2(1999), 177-179.

(6) Charge Variation Effects on Ion Acoustic Waves in Dusty Plasmas
T. Takaishi and K. Nishikawa
Journal of Physical Society Japan, 68 (1999), No.9, 2962-2964.

(7) Connecting Orbit Structure of Monotone Solutions in the Shadow System
H. Kokubu, K. Mischaikow, Y. Nishiura, H. Oka and T. Takaishi
Journal of Differential Equations, 140 (1997), 309—364.

(8) Dynamics of Inhibitory Pulse-coupled Oscillators
Y. Nishiura, J. Shidawara, and T. Takaishi
Dynamical Systems and Applications 4 (1995),549—561,World Scientific.

主論文

Abstract

The bifurcation structures of two types of reaction diffusion systems are investigated.

A phase field model for anti-plane shear crack growth in two dimensional isotropic elastic material is proposed. A phase field to represent the shape of the crack with a regularization parameter $\epsilon > 0$ is introduced. The phase field model is derived as a gradient flow of this regularized energy that is approximated by the Francfort-Marigo type energy using the idea of Ambrosio and Tortorelli. Several numerical examples of the crack growth computed with an adaptive mesh finite element method are presented.

A simplified coupled reaction-diffusion system is derived from a diffusive membrane coupling of two reaction-diffusion systems of activator-inhibitor type. It is shown that the dynamics of the original decoupled systems persists for weak coupling, while new coupled *stationary* patterns of *alternated* type emerge at a critical strength of coupling and these become stable for strong coupling independently of the dynamics of the decoupled systems. The approach which is used here is singular perturbation techniques and complementarily numerical methods.

In this Thesis, the usefulness of the combination of the mathematical modeling and the numerical simulation for investigating the bifurcation phenomena on the nonlinear pattern formation in reaction diffusion system is found.

Keywords: reaction-diffusion system, crack growth, phase field model, Turing pattern, diffusive coupling, numerical simulation
AMS Subject Classification: 74R10, 35K57, 81T80

Contents

Chapter 1

Reaction Diffusion System and Bifurcation Phenomena

1.1 Reaction Diffusion System

Reaction diffusion systems raise the great interests in nonlinear phenomena. Focusing on the spatio-temporal pattern formation, reaction diffusion systems were appllied to the texture on animal skin, population and distribution dynamics of the biological system, mutual interaction on nerval matrix of coral system, to name a few.

The simplicity of the structure would be the reason why reaction-diffusion system has had great interests on many genre (or category) of nonlinear phenomena that posess various kind of complexity in it. With some ingenuity, we are able to build a mathematical model that has the expression of reaction-diffusion sysytem which is easily handled by analytical and numerical approaches.

In this thesis, two types of reaction diffusion system are treated. Both of them consist of the reaction-diffusion equations on two scalar variables u and v.

$$\begin{cases} \alpha_1 \dfrac{\partial u}{\partial t} &= \operatorname{div}(d_u \nabla u) + f(u,v) \\ \alpha_2 \dfrac{\partial v}{\partial t} &= \operatorname{div}(d_v \nabla v) + g(u,v) \\ &+ \ (\text{BoundaryConditions}) \end{cases} \tag{1.1}$$

Diffusion systems with nonlinear reaction terms have multiple solutions in many case. Taking up the two types of reaction-diffusion system, the author investigate the bifurcation structure of their dynamics in this thesis.

Chapter 2 treats spatial patterns arising from crack evolutions on a elastic plate. In usual, the path of crack evolution is investigated by the energy estimation of its system, however, artificial conditions for numerical scheme are assumed in many cases. The author and Kimura introduce a kind of the reaction-diffusion equations that describes the force balance of the media and the phase field of crack and damage. Investigating these equations, the paths of cracks are categorized by the initial cracks without any artificial condition of on the numerical simulation.

In Chapter 3, spatio-temporal patterns found in mutual interaction between 2 sheets of reaction-diffusion system are treated. Each system has potential to make spatio-temporal pattern, the Turing-like instability is found when 2 sheets have mutual interaction via diffusive membrane coupling. This coupled-RD system has an analogy of the interaction between the pattern dynamics. Stationary and oscilattory pattern are treated here.

Chapter 2

Crack Evolution

2.1 Crack Evolution of Isotropic Elastic Plate

We propose the following mathematical model for the mode III (anti-plane shear mode) crack growth in an elastic plate. Let Ω be a bounded two dimensional domain with a piecewise smooth boundary Γ, and let Γ_D be a nonempty open portion of Γ which consists of a finite number of connected

components. For $t > 0$, we consider the equations

$$\begin{cases} \alpha_1 \dfrac{\partial u}{\partial t} &= \operatorname{div}\left((1-z)^2 \nabla u\right) & x \in \Omega \\ \alpha_2 \dfrac{\partial z}{\partial t} &= \left(\varepsilon \Delta z - \dfrac{\gamma^2}{\varepsilon} z + |\nabla u|^2 (1-z)\right)_+ & x \in \Omega \\ u(x,t) &= g(x,t) & x \in \Gamma_D \\ \dfrac{\partial u}{\partial n} &= 0 & x \in \Gamma_N \\ \dfrac{\partial z}{\partial n} &= 0 & x \in \Gamma \\ + \text{ I.C. (2.2)} & & x \in \Omega, \end{cases} \tag{2.1}$$

where $\Gamma_N := \Gamma \backslash \Gamma_D$ and $u(x,t)$ represents the small anti-plane displacement at the position $x \in \overline{\Omega}$ and time $t \geq 0$, and $g(x,t)$ is a given anti-plane displacement on the boundary Γ_D. The variable $z(x,t)$ satisfies $0 \leq z(x,t) \leq 1$ in Ω and represents the crack shape, as $z \approx 0$ in the region without crack and $z \approx 1$ near the crack. The minimum length scale of z is given as $O(\varepsilon)$ with a small regularization parameter $\varepsilon > 0$. The function $z(x,t)$ is called the phase field for the crack shape. For stable numerical simulations, we also introduce small time relaxation parameters $\alpha_1 \geq 0$ and $\alpha_2 > 0$. The initial conditions for (2.1) are given as follows:

$$\begin{cases} u(x,0) &= u_0(x) & x \in \Omega \quad (\text{omitted if } \alpha_1 = 0) \\ z(x,0) &= z_0(x) \in [0,1] & x \in \Omega \end{cases} \tag{2.2}$$

The first equation of (2.1) expresses the force balance in the uncracked region ($z \approx 0$), and the second equation expresses the crack evolution due

to the modulus of the stress $|\nabla u|$. The material constant $\gamma > 0$ is called the fracture toughness, which prescribes the critical value of the energy release rate in the Griffith's criterion. It is harder for the crack to grow, if the value of γ is larger.

A crack once generated can be no longer repaired. We put $(\ )_+$ to the right hand side of the second equation, where $(a)_+ = \max(a, 0)$. It guarantees the non-repair condition for the crack: $\frac{\partial z}{\partial t} \geq 0$.

The derivation of this mathematical model is shown in Section 2.3, and some computational results will be given in Section 2.4.

2.2 Three modes of crack evolution and the fundamental equations of elastic media

Crack evolution is found in a various place, wall, structure, body, ground, and etc. Investigation of the crack has a long history, because we recognize that the crack induce the serious damage of the materials.

Numerical simulation of the crack evolution problem has actually many difficulties. One is the singularity of the stress concentration at the tip of the crack. Classical theory of the crack evolution tells us that the gradient of the displacement of material becomes infinity at the tip, then, difficulty on the numerical treatment at the tip is inevitable. The second is the lack of the explicit method for selecting the direction of the crack evolution. We need the energy evaluation for all directions every time the crack is elongated. The method of the selection of the direction and the cost of computation induces the difficulty to solve this problem. The third is difficulty for treating the

new cracks or subcracks. For estimating the energy, it is necessary to check the new cracks everywhere except the tip. The fourth, to remesh for new boundaries that crack evoution make is the essential task for computation. If one assumes the crack line as a new boundary, the shape of the computational region changes according to the crack evolution. Then, we need to restart the computation for the new shape of the mesh, it costs very much. Many schemes have been developed for solving these problem ([9],etc.). We derived the temporal evolution equation of the reaction-diffusion type with phase field for describing the cracked region.

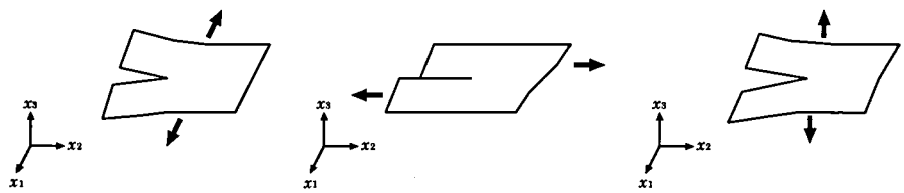

(a) (b) (c)

Figure 2.1: Three types of crack evolution.(a) mode I, (b) mode II, and (c) mode III

The crack evolution on the plate is classified into three types by the direction of the stress (Figure 2.1) . Using the phase field, we introduce the mathematical model of the mode III crack evolution that is free from the computational difficulties mentioned above.

In the classical theory of linear elasticity, the strain-displacement equation in cartesian coordinate is written as

$$\sigma_{ij} = \frac{1}{2}\left(\frac{\partial u_i}{\partial x_j} + \frac{\partial u_j}{\partial x_i}\right), \tag{2.3}$$

where σ_{ij} is the strain tensor and u_i is the displacement vector. When Hook's law is introduced in isotropic media, stress tensor T_{ij} is written as follows

$$\begin{cases} T_{ij} &= C_{ijkl}\sigma_{kl} \\ C_{ijkl} &= \lambda\delta_{ij}\delta_{kl} + \mu\left(\delta_{ik}\delta_{jl} + \delta_{il}\delta_{jk}\right) \end{cases}, \tag{2.4}$$

where C_{ijkl} are the coefficients of the elasticity tensor, λ and μ are Lame's constants. Then (2.4) is rewrite as

$$\begin{aligned} T_{ij} &= C_{ijkl}\sigma_{kl} \\ &= \left\{\lambda\delta_{ij}\delta_{kl} + \mu\left(\delta_{ik}\delta_{jl} + \delta_{il}\delta_{jk}\right)\right\}\sigma_{kl} \\ &= \lambda\delta_{ij}\sigma_{kk} + \mu\left(\sigma_{ij} + \sigma_{ji}\right) \\ &= \lambda\delta_{ij}\mathrm{div}(u) + 2\mu\sigma_{ij}. \end{aligned} \tag{2.5}$$

The balance equation of stress and body force f is

$$\frac{\partial t_{ij}}{\partial x_j} + f_i = 0. \tag{2.6}$$

The bulk energy of domain Ω, E, is written as follows

$$\begin{cases} E &= \int_\Omega w dx \\ w &= \frac{1}{2} T_{ij}\sigma_{ij} \end{cases} \tag{2.7}$$

where w is the energy density.

When the plate in the two dimensional domain $\Omega \in (x_1, x_2)$ is subjected to only the anti-plate displacement in x_3-direction, the displacement vector

becomes $u = (0, 0, u_3(x_1, x_2))$ and div$u = 0$ (mode III type, Figure 2.1).

$$T = \mu \begin{pmatrix} 0 & 0 & \dfrac{\partial u_3}{\partial x_1} \\ 0 & 0 & \dfrac{\partial u_3}{\partial x_2} \\ \dfrac{\partial u_3}{\partial x_1} & \dfrac{\partial u_3}{\partial x_2} & 0 \end{pmatrix} \tag{2.8}$$

The balance equation for (2.8) is

$$0 = \mu \left(\frac{\partial t_{31}}{\partial x_1} + \frac{\partial t_{32}}{\partial x_2} \right) + f_3 = \mu \left(\frac{\partial^2}{\partial x_1^2} + \frac{\partial^2}{\partial x_2^2} \right) u_3 + f_3 \tag{2.9}$$

and the bulk energy density is defined as

$$w = \frac{\mu}{2} \left(\left(\frac{\partial u_3}{\partial x_1} \right)^2 + \left(\frac{\partial u_3}{\partial x_2} \right)^2 \right) = \frac{\mu}{2} |\nabla u_3|^2 . \tag{2.10}$$

Then, the total bulk energy of mode III crack evolution is given by

$$E = \frac{\mu}{2} \int_\Omega |\nabla u_3|^2 \, dx. \tag{2.11}$$

2.3 Griffith's criterion and the phase field model of the mode-III crack growth

A crack propagation in a plate by the deformation perpendicular to the plate is considered. Let Ω be a bounded two dimensional domain as described in Section 2.1. $x = (x_1, x_2) \in \mathbb{R}^2$ stands for the Cartesian coordinate parallel to the plate, and x_3 is the coordinate perpendicular to the plate. The plate is assumed to be an isotropic elastic material with a constant thickness and is treated as a two dimensional domain Ω.

A crack in the plate Ω is denoted by a closed subset $\Sigma \subset \Omega$. It is assumed that the deformation of the plate is limited to the x_3-direction, and the anti-plane displacement is denoted by $u(x) \in \mathbb{R}$ for $x \in \Omega \backslash \Sigma$. If the speed of the crack evolution is very slow, we may adapt the quasi-static assumption, saying that the following equations are valid for every fixed t:

$$\begin{cases} -\mu \Delta u = f & \text{in} \quad \Omega \backslash \Sigma \\ u = g & \text{on} \quad \Gamma_D \\ \mu \dfrac{\partial u}{\partial n} = h & \text{on} \quad \Gamma_N \\ \dfrac{\partial u^{\pm}}{\partial n} = 0 & \text{on} \quad \Sigma^{\pm}, \end{cases} \tag{2.12}$$

where $f(x)$ is a given external load perpendicular to the plate on Ω, $g(x)$ is a given anti-plane displacement on Γ_D, and $h(x)$ is a given boundary load in the x_3-direction on Γ_N. The outward normal derivative on the boundary of $\Omega \backslash \Sigma$ is denoted by $\frac{\partial}{\partial n}$. In particular, $\frac{\partial u^+}{\partial n}$ and $\frac{\partial u^-}{\partial n}$ stand for the outward normal derivatives of u on the sides Σ^+ and Σ^-, respectively, where the both sides of the crack Σ are denoted by Σ^+ and Σ^-. The parameter $\mu > 0$ measures the rigidity, which is one of the Lamé constants.

The solution u to (2.12) is obtained as a unique minimizer of the following elastic potential energy including the external loads:

$$E_1(v, \Sigma) = \frac{\mu}{2} \int_{\Omega \backslash \Sigma} |\nabla v|^2 \, dx - \int_{\Omega} f v \, dx - \int_{\Gamma_N} h v \, ds \qquad (v \in V(g, \Omega \backslash \Sigma)),$$

where $V(g, \Omega \backslash \Sigma) := \{v \in H^1(\Omega \backslash \Sigma);\ v = g \text{ on } \Gamma_D\}$. We have assumed that $g = \tilde{g}|_{\Gamma_D}$ with $\tilde{g} \in H^1(\Omega)$ and that $h \in L^2(\Gamma_N)$.

According to the classical theory of brittle fracture by A. A. Griffith [8], the elastic energy which is released along the crack evolution is the source

of energy supply for creating new cracks. Francfort-Marigo [7] proposed the following energy based on the Griffith's theory:

$$\begin{cases} E(\Sigma) &= E_1(u,\Sigma) + E_2(\Sigma), \\ E_1(u,\Sigma) &= \min\limits_{v \in V(g,\Omega\backslash\Sigma)} E_1(v,\Sigma) \qquad (u \in V(g,\Omega\backslash\Sigma)), \\ E_2(\Sigma) &:= \int_\Sigma \gamma(x)\, ds. \end{cases} \tag{2.13}$$

The total energy of our system E, which is called the free energy in the analogy of the time dependent Ginzburg-Landau (TDGL) theory or the phase field model approach ([12] etc.), is given as the sum of the elastic potential energy E_1 over $\Omega\backslash\Sigma$ and a surface energy E_2 on the crack. At a time t, the bulk energy $E_1(u,\Sigma)$ which is generated by the strain of the elastic plate is given as the minimum potential energy of E_1.

Let us suppose that a crack Σ grows and becomes $\tilde{\Sigma}(\supset \Sigma)$. Since $V(g,\Omega\backslash\Sigma) \subset V(g,\Omega\backslash\tilde{\Sigma})$,

$$E_1(u,\Sigma) = \min_{v \in V(g,\Omega\backslash\Sigma)} E_1(v,\tilde{\Sigma}) \geq \min_{v \in V(g,\Omega\backslash\tilde{\Sigma})} E_1(v,\tilde{\Sigma}) = E_1(\tilde{u},\tilde{\Sigma}),$$

holds. The released potential energy $E_1(u,\Sigma) - E_1(\tilde{u},\tilde{\Sigma}) \geq 0$ along the crack growth from Σ to $\tilde{\Sigma}$ is used to reduce the surface energy E_2 depending on the fracture toughness $\gamma(x) > 0$.

In [7], a mathematical model for crack growth with this energy is proposed and studied in detail. In practical numerical computations, however, we have the following numerical difficulties: 1) numerical treatment of stress concentration at the crack tip (i.e. $|\nabla u| = \infty$), 2) no explicit formula for crack path determination, 3) numerical treatment of crack initiation or sub-

cracks, 4) numerical task to re-mesh $\Omega\backslash\Sigma(t)$ for the finite element method or other numerical methods.

In order to represent the crack shape, we consider a phase field $z(x)$, which satisfies $z \approx 1$ around the crack and $z \approx 0$ for the other region. Introducing a sufficiently small spatial regularization parameter $\epsilon > 0$, we suppose that the crack has $O(\epsilon)$ thickness. Let $\mathcal{E}_1(u,z)$ and $\mathcal{E}_2(z)$ be approximations of the bulk energy $E_1(u,\Sigma)$ and the surface energy $E_2(\Sigma)$, respectively. Using the idea of Ambrosio-Tortorellio [1], we consider the following regularized energy which depends on the anti-plane displacement $u \in V(g,\Omega)$ and the phase field for the crack shape $z \in H^1(\Omega)$ with $0 \le z(x) \le 1$:

$$\begin{cases} \mathcal{E}(u,z) &:= \mathcal{E}_1(u,z) + \mathcal{E}_2(z) \\ \mathcal{E}_1(u,z) &:= \dfrac{\mu}{2}\displaystyle\int_\Omega (1-z)^2 |\nabla u|^2 \, dx - \int_\Omega fu \, dx - \int_{\Gamma_N} (1-z)^2 hu \, ds \\ \mathcal{E}_2(z) &:= \dfrac{1}{2}\displaystyle\int_\Omega \gamma(x) \left(\epsilon |\nabla z|^2 + \frac{1}{\epsilon} z^2 \right) dx \end{cases} \tag{2.14}$$

In [1], it is mathematically proved that this energy approximates (2.13) as $\epsilon \to 0$ in the sense of Γ-convergence.

We suppose that the given external force f, h and the given boundary displacement g change slowly in time and that u and z approach the (quasi-)equilibrium state in relatively smaller time scales. In the TDGL theory or the phase field approach, the dynamics near equilibrium of a system is described by the gradient flow of the free energy (see [12] etc.). In general, for a free energy $F(u)$, its gradient flow is given by $\alpha \frac{\partial u}{\partial t} = -\frac{\delta F}{\delta u}$, where $\alpha > 0$ is a suitable time constant and $\frac{\delta F}{\delta u}$ is the first variation of F with respect to u.

Let us make a brief comment on the gradient flow of energy $F(u)$ by TDGL. We set that $F(u)$ is a function in R^2. The change of $F(u+\rho\zeta)$ at $\rho = 0$ for u fixed is given by

$$\frac{d}{d\rho}F(u+\rho\zeta)\Big|_{\rho=0} = \nabla F(u)\cdot\zeta,$$

where $\nabla F(u)$ is the gradient of the function $F(u)$ and it describes the gradient of energy flow. When we assume that the dynamics of $u(t)$ evolves as descending the energy with the speed proportional to $|\nabla F(u)|$, the equation of u is given by

$$\begin{cases} \alpha\dfrac{\partial u}{\partial t} &= -\nabla F(u) \\ \dfrac{d}{d\rho}F(u+\rho\zeta)\Big|_{\rho=0} &= \nabla F(u)\cdot\zeta. \end{cases} \tag{2.15}$$

Suppose that $\Gamma_N = \Gamma_N^0 \cup \Gamma_N^1, \Gamma_N^0 \cap \Gamma_N^1 = \emptyset$ and that $h = 0$ on Γ_N^0. We assume that h may not vanish on Γ_N^1 and the crack does not touch the boundary Γ_N^1. We assume the following conditions:

$$\begin{cases} u = g & \dfrac{\partial z}{\partial n} = 0 \quad \text{on} \quad \Gamma_{\mathrm{D}} \\ \mu\dfrac{\partial u}{\partial n} = h = 0 & \dfrac{\partial z}{\partial n} = 0 \quad \text{on} \quad \Gamma_{\mathrm{N}}^0 \\ \mu\dfrac{\partial u}{\partial n} = h & z = 0 \quad \text{on} \quad \Gamma_{\mathrm{N}}^1 \end{cases} \tag{2.16}$$

Calculating the energy gradient of this system. The boundary conditions are set so that $u = g$ on Γ_D, $\frac{\partial u}{\partial n} = 0$ on Γ_N. We now compute the first

variation of the energy in (2.14). For any $\xi \in V(0,\Omega)$,

$$\begin{aligned} \frac{d}{d\rho}\mathcal{E}(u+\rho\xi,z)\Big|_{\rho=0} &= \frac{d}{d\rho}\mathcal{E}_1(u+\rho\xi,z)\Big|_{\rho=0} \\ &= \mu\int_\Omega (1-z)^2\nabla u\cdot\nabla\xi\,dx - \int_\Omega f\xi\,dx. \end{aligned} \tag{2.17}$$

From the boundary condition at Γ, the first term is rewriten as follows:

$$\begin{aligned} \mu\int_\Omega (1-z)^2\nabla u\cdot\nabla\xi\,dx &= \mu\int_\Gamma (1-z)^2\frac{\partial u}{\partial n}\xi\,ds - \mu\int_\Omega \mathrm{div}\left((1-z)^2\nabla u\right)\xi\,dx \\ &= -\mu\int_\Omega \mathrm{div}\left((1-z)^2\nabla u\right)\xi\,dx, \end{aligned}$$

from which we obatain

$$\frac{d}{d\rho}\mathcal{E}(u+\rho\xi,z)\Big|_{\rho=0} = -\int_\Omega \left\{\mu\,\mathrm{div}\left((1-z)^2\nabla u\right)+f\right\}\xi\,dx. \tag{2.18}$$

Then, the gradient flow of the energy (2.14) with respect to u becomes

$$\alpha_1\frac{\partial u}{\partial t} = \mu\,\mathrm{div}\left((1-z)^2\nabla u\right)+f. \tag{2.19}$$

We remark that $\alpha_1 = 0$ corresponds to the original quasi-static assumption in (2.12) and the case with $0 < \alpha_1 << 1$ is considered as its natural approximation. Actually, in case of $\alpha_1 = 0$, the elliptic equation degenerates if $z = 1$ and a small time constant $\alpha_1 > 0$ is effective to stabilize its numerical computation.

Similarly, under these conditions we have the gradient flow for $z(x,t)$ with

a suitable time constant $\alpha_2 > 0$:

$$\begin{aligned}
\frac{d}{d\rho}\mathcal{E}_1(u, z+\rho\zeta)\Big|_{\rho=0} &= -\mu\int_\Omega (1-z)|\nabla u|^2\zeta\, dx \\
\frac{d}{d\rho}\mathcal{E}_2(z+\rho\zeta)\Big|_{\rho=0} &= \int_\Omega \gamma(x)\left(\epsilon\nabla z\cdot\nabla\zeta + \frac{1}{\epsilon}z\zeta\right) dx \\
&= \epsilon\left\{\int_\Gamma \gamma(x)\frac{\partial z}{\partial n}\zeta\, ds - \int_\Omega \operatorname{div}(\gamma(x)\nabla z)\,\zeta\, dx\right\} + \int_\Omega \gamma(x)\frac{1}{\epsilon}z\zeta\, dx \\
&= -\int_\Omega \left\{\epsilon\operatorname{div}(\gamma(x)\nabla z) - \frac{\gamma(x)}{\epsilon}z\right\}\zeta\, dx
\end{aligned} \tag{2.20}$$

then, the following equation is obtained.

$$\frac{d}{d\rho}\mathcal{E}(u, z+\rho\zeta)\Big|_{\rho=0} = -\int_\Omega \left\{\epsilon\operatorname{div}(\gamma(x)\nabla z) - \frac{\gamma(x)}{\epsilon}z + \mu|\nabla u|^2(1-z)\right\}\zeta\, dx \tag{2.21}$$

Using the appropriate time constant $\alpha_2 > 0$, the energy flow for the phase field z is written as follows:

$$\alpha_2\frac{\partial z}{\partial t} = \epsilon\operatorname{div}(\gamma(x)\nabla z) - \frac{\gamma(x)}{\epsilon}z + \mu|\nabla u|^2(1-z) \tag{2.22}$$

From the non-recovable nature of crack, it is reasonable to set

$$\frac{\partial z}{\partial t} \geq 0. \tag{2.23}$$

Although there are many possibilities to realize this condition, $\alpha_2\frac{\partial z}{\partial t} = (\cdots)_+$ is adoptted here, where $(a)_+ = \max(a, 0)$. Then, following equation is obtained from (2.22).

$$\alpha_2\frac{\partial z}{\partial t} = \left(\epsilon\operatorname{div}(\gamma(x)\nabla z) - \frac{\gamma(x)}{\epsilon}z + \mu|\nabla u|^2(1-z)\right)_+ \tag{2.24}$$

Summarizing (2.19) and (2.24), we obtain the following phase field model for crack growth:

$$\begin{cases} \alpha_1 \dfrac{\partial u}{\partial t} &= \mu \operatorname{div}\left((1-z)^2 \nabla u\right) + f(x,t) & x \in \Omega \\ \alpha_2 \dfrac{\partial z}{\partial t} &= \left(\epsilon \operatorname{div}\left(\gamma(x)\nabla z\right) - \dfrac{\gamma(x)}{\epsilon} z + \mu |\nabla u|^2 (1-z)\right)_+ & x \in \Omega \\ + \text{ B.C. (2.16)} \\ + \text{ I.C. (2.2).} \end{cases} \tag{2.25}$$

In the second equation, to guarantee the non-repair condition for the crack ($\frac{\partial z}{\partial t} \geq 0$), we have modified (2.22) as $\alpha_2 \frac{\partial z}{\partial t} = (\cdots)_+$, where $(a)_+ = \max(a, 0)$. A class of such evolution equations with constraint is studied mathematically in [14]. Similar approaches for computing the Francfort-Marigo model with regularized energy are found in [2, 3, 4, 5].

In (2.25), setting $\Gamma_N^0 = \Gamma_N, f = 0, \gamma(x) \equiv \gamma > 0, \mu = 1$ and replacing $\epsilon\gamma$ by ε, we obtain (2.1). This model no longer has any numerical difficulties for computer simulation. Several numerical results is shown in the next section.

Finally, we estimate the temproal evolution of the total energy of the system which the phase field model describes, when h, f and g are constant in time. From the quasi-static assumption, the time-evolutions of u and z are assumed to be slower than the variation of the energy ($\frac{\partial f}{\partial t} = 0, \frac{\partial g}{\partial t} = 0$),

and we can compute $\frac{d}{dt}\mathcal{E}_1$ and $\frac{d}{dt}\mathcal{E}_2$ as follows:

$$\begin{aligned}
\frac{d}{dt}\mathcal{E}_1(u,z) &= \mu\int_\Omega \left\{-(1-z)\left|\nabla u\right|^2\frac{\partial z}{\partial t} + (1-z)^2\nabla u\cdot\nabla\frac{\partial u}{\partial t}\right\}dx - \int_\Omega f\frac{\partial u}{\partial t}\,dx \\
&= -\mu\int_\Omega (1-z)\left|\nabla u\right|^2\frac{\partial z}{\partial t}\,dx + \mu\int_\Gamma (1-z)^2\frac{\partial u}{\partial n}\frac{\partial u}{\partial t}\,ds \\
&\quad -\mu\int_\Omega \operatorname{div}\left((1-z)^2\nabla u\right)\frac{\partial u}{\partial t}\,dx - \int_\Omega f\frac{\partial u}{\partial t}\,dx \\
&= -\mu\int_\Omega (1-z)\left|\nabla u\right|^2\frac{\partial z}{\partial t}\,dx - \int_\Omega \left\{\mu\operatorname{div}\left((1-z)^2\nabla u\right)+f\right\}\frac{\partial u}{\partial t}\,dx
\end{aligned} \tag{2.26}$$

For $\mathcal{E}_2$,

$$\begin{aligned}
\frac{d}{dt}\mathcal{E}_2(z) &= \int_\Omega \gamma(x)\left\{\epsilon\,\nabla z\cdot\nabla\frac{\partial z}{\partial t} + \frac{1}{\epsilon}z\frac{\partial z}{\partial t}\right\}dx \\
&= \int_\Gamma \epsilon\,\gamma(x)\frac{\partial z}{\partial n}\frac{\partial z}{\partial t}\,ds - \int_\Omega \epsilon\operatorname{div}\left(\gamma(x)\nabla z\right)\frac{\partial z}{\partial t}\,dx + \int_\Omega \frac{\gamma(x)}{\epsilon}z\frac{\partial z}{\partial t}\,dx \\
&= -\int_\Omega \left\{\epsilon\operatorname{div}\left(\gamma(x)\nabla z\right) - \frac{\gamma(x)}{\epsilon}z\right\}\frac{\partial z}{\partial t}\,dx.
\end{aligned} \tag{2.27}$$

One can see that the temporal evolution of the total energy of this system has the feature of dissipative system as follows:

$$\frac{d}{dt}\mathcal{E}(u,z) = -\int_\Omega \left(\alpha_1\left|\frac{\partial u}{\partial t}\right|^2 + \alpha_2\left|\frac{\partial z}{\partial t}\right|^2\right)dx \le 0 \tag{2.28}$$

Notice that (2.28) holds not only in the case of (2.22), but also (2.25) with $\alpha_2\frac{\partial z}{\partial t} = (\cdots)_+$.

2.4 Numerical simulation

2.4.1 Numerical scheme

In this section, we exhibit numerical simulation performed with FEM on adaptive-mesh. An adaptive mesh finite element solver was used for reaction diffusion systems in [10, 11] with an adaptive mesh FEM toolbox ALBERTA [13] .

Let $u^k(x)$ and $z^k(x)$ be the approximations of u and z at $t = k\tau$ ($k = 0, 1, 2, \cdots$), respectively, with time increment $\tau > 0$. To obtain u^k and z^k from u^{k-1} and z^{k-1}, the following implicit scheme for the first two equations of (2.25) is adopted:

$$\begin{cases} \alpha_1 \dfrac{u^k - u^{k-1}}{\tau} &= \mu \operatorname{div}\left((1 - z^{k-1})^2 \nabla u^k\right) \\ \alpha_2 \dfrac{\tilde{z}^k - z^{k-1}}{\tau} &= \epsilon \operatorname{div}\left(\gamma(x) \nabla \tilde{z}^k\right) - \dfrac{\gamma(x)}{\epsilon} \tilde{z}^k + \mu |\nabla u^{k-1}|^2 (1 - \tilde{z}^k) \\ z^k &= \max(\tilde{z}^k,\, z^{k-1}) \end{cases} \tag{2.29}$$

Here, we set $y = \min(\tilde{z}^k, 0)$ and integrate the second equation, then

$$\int_\Omega \left\{ 1 + \frac{\tau}{\alpha_2} \left(\frac{\gamma(x)}{\epsilon} + \mu |\nabla u^{k-1}|^2 \right) \right\} \tilde{z}^k y \, dx + \int_\Omega \frac{\epsilon\tau}{\alpha_2} \nabla \tilde{z}^k \cdot \nabla y \, dx = \int_\Omega \left(z^{k-1} + \frac{\tau\mu}{\alpha_2} |\nabla u^{k-1}|^2 \right) y \, dx$$

is obtained, and almost everywhere, $y \leq 0$ and $\tilde{z}^k y = y^2, \nabla \tilde{z}^k \cdot \nabla y = |\nabla y|^2$,

$$\int_\Omega \left\{ 1 + \frac{\tau}{\alpha_2} \left(\frac{\gamma(x)}{\epsilon} + \mu |\nabla u^{k-1}|^2 \right) \right\} y^2 \, dx + \int_\Omega \frac{\epsilon\tau}{\alpha_2} |\nabla y|^2 \, dx = \int_\Omega \left(z^{k-1} + \frac{\tau\mu}{\alpha_2} |\nabla u^{k-1}|^2 \right) y \, dx.$$

If $z^{k-1} \geq 0$, (R.H.S) ≤ 0 leads to $y = 0$, and hence $\tilde{z}^k \geq 0$ follows. Similar calculations on $\zeta = 1 - z^{k-1}$, $z^{k-1} \leq 1$ leads to $\tilde{z}^k \leq 1$. Then, when the initial value z^0 satisfies $0 \leq z^0 \leq 1$, $0 \leq z^k \leq 1$ is guaranteed.

The condition $\tilde{z}^k \in [0, 1]$ is derived by the maximum principle for elliptic equations for $\tilde{z}^k$, and it leads to $z^k \in [0, 1]$. In this paper, the simple scheme (2.29) with sufficiently small τ is adopted. It will be interesting, however, to apply the projected SOR method [6] to the second equation of (2.25) for more accurate computation.

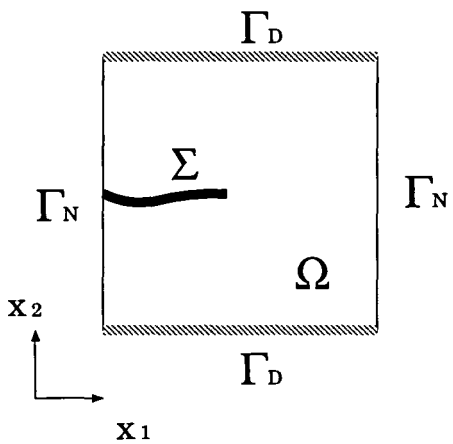

Figure 2.2: Computational domain

We solve (2.29) by using the adaptive mesh FEM with $P1$ elements and adaptive time step control (see [10, 11]). In the following simulations, we put $\epsilon = 10^{-3}, \alpha_1 = 0, \alpha_2 = 10^{-3}$ in (2.25), and set the computational domain as $\Omega = (-1, 1) \times (-1, 1)$ with $\Gamma_D = \{(x_1, x_2) | x_1 \in (-1, 1), x_2 = \pm 1, \}$ (Figure 2.2). The boundary condition for u is given by $g(x, t) = 10 x_2 t$ for $x \in \Gamma_D$ and $t \geq 0$.

	max(mesh number)	min(mesh size)	min(τ)	max (τ)
i)	8192	0.005524	0.001477	0.089005
ii)	40824	0.001953	0.001407	0.066417
iii) (a)	18496	0.002762	0.001477	0.063254
iii) (b)	17788	0.002762	0.001477	0.069738
iv) (a)	128856	0.001953	0.001407	0.088783
iv) (b)	114264	0.000691	0.001407	0.098128

Table 2.1: Computational data on adaptive mesh

Four cases with different γ and $z_0(x)$ are considered. The fracture toughness γ is set to be constant in the first three cases, and variable $\gamma = \gamma(x)$ is treated in the last case.

Table 2.1 shows the computational data on adaptive mesh for these numerical simulations.

2.4.2 One crack evolution ($\gamma = 0.5$)

One straight crack in the plate is set at $t = 0$. The initial condition for z is defined by $z_0(x) := \zeta_0(x_1 + 0.5, x_2)$, where $\zeta_0(x) := e^{-(x_2/\delta)^2}(1 + e^{x_1/\delta})^{-1}$ with $\delta = 0.1$. (In the other simulations of this section, initial conditions are also defined similarly with suitable shift and superposition of the above $\zeta_0(x)$.)

It can be seen that the crack grows straight and reaches the right-hand

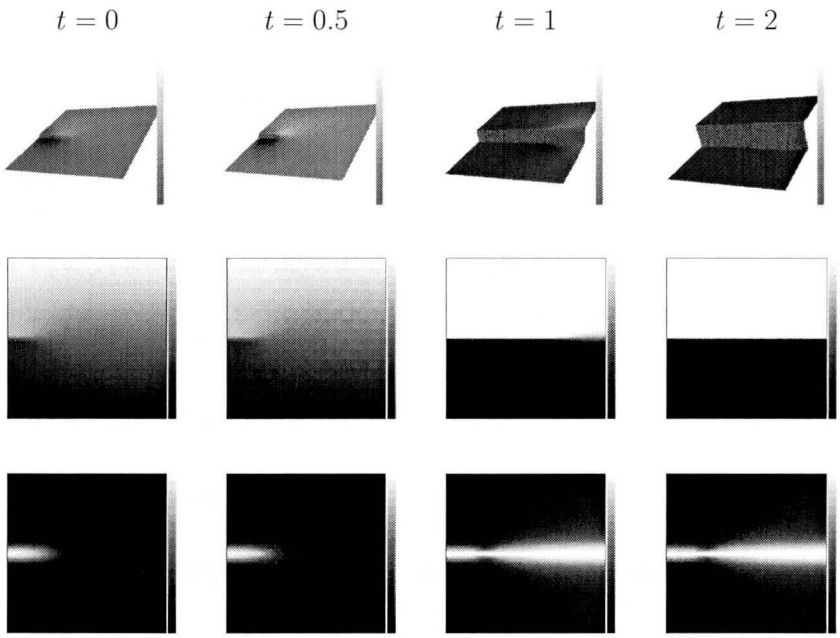

Figure 2.3: Bird's-eye views of u(top), u (middle) and z (bottom) in the temporal crack evolution.

side boundary (Figure 2.3). Bird's-eye views of displacement u are shown at top, graphs in the middle show the distribution of u (middle) which are normalized by its maximum and minimum values. Graphs of u shows that the deformation of u is recovered after the growth of crack. Intensity of the graphs at the bottom shows the value of z, $z = 0$ as black, $z = 1$ as white, and the temporal growth of the crack domain ($z \approx 1$: white) is shown there. For reference, all the graphs have the color-bar (grey-scale) at the right-hand side of them. As the crack grows, the region $z > 0$ grows wider than $o(\epsilon)$, because

the model is implicitly defined that the history of the deformation makes the plate damaged. Once the plate is damaged, repair of damage of the deformed material (ex. deviation of atomic coodination) needs the long time although the deformation is recovered soon. In this model, this effect is shown as the width of $z > 0$ from the positiveness of z_t ($z_t = (F(u,z))_+ \geq 0$), and the numerical reults shows that the region $z > 0$ changes its width according to the functional of $\phi(x)$ of $z_t = \phi(F)$. In this model, mendingless assumption of the damage ($\phi(x) = x_+$) leads to the result that the width of the region $z > 0$ becomes larger where the deformation stays longer.

It is confirmed that this numerical result is supported by the mesh adaptation. From the result of the numerical simulation, the minimum mesh size reaches the smallest when the crack evolution starts ($t \sim 0.5$ in Figure 2.5), the total number of the computational mesh increments after that. The total number of the mesh saturates when the crack reaches the opposite bundary. Figures 2.4 and 2.5 shows how the mesh adaptation works on this numerical simulation (Figure 2.3), and that it is possible to calculate this problem on the fixed mesh when $h \sim 0.003$ is employed.

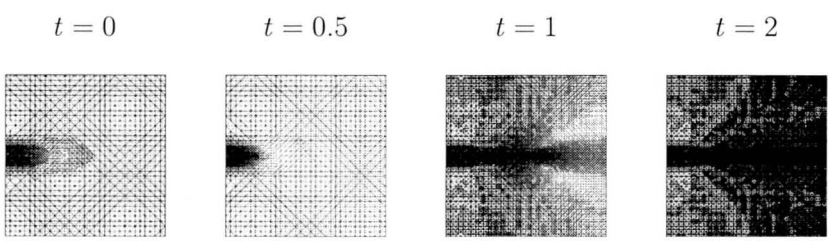

Figure 2.4: Adaptive mesh in the temporal crack evolution.

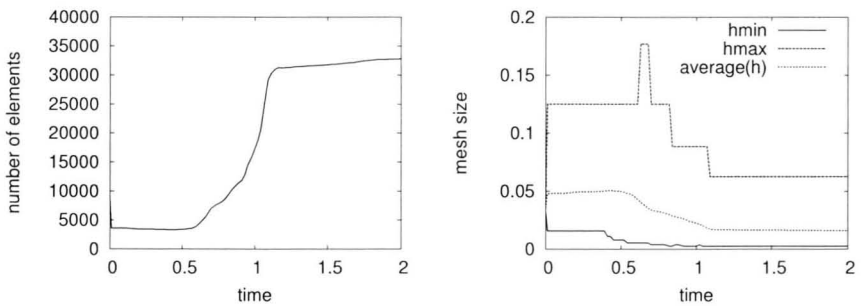

Figure 2.5: Temporal evolution of the number of elements (left) and mesh size (right).

2.4.3 Sub-crack and bifurcation behaviour for growing two cracks

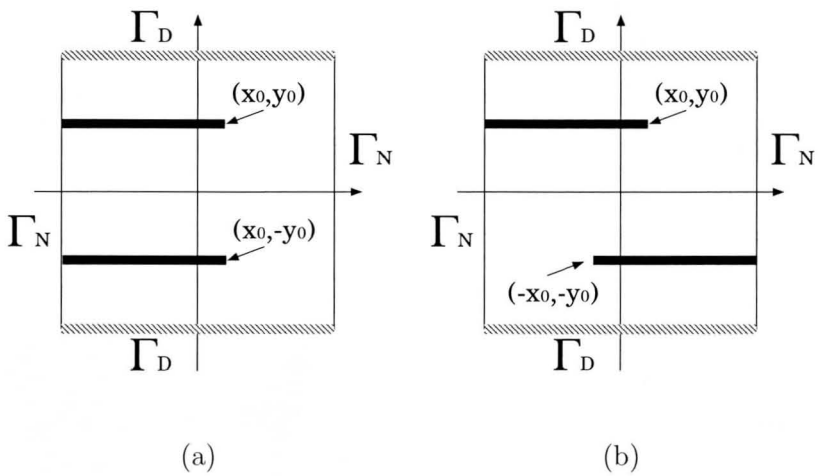

Figure 2.6: Computational domain and initial 2 cracks in the case i) (a) and the case ii) (b).

i) Two cracks in the same direction ($\gamma = 0.5$)

At $t = 0$ two cracks on the left-hand side boundary with the same length is set. If the length is long enough, they reach to the right-hand side boundary. They, however, merge into one crack when the length of the two cracks is not enough long (Figure 2.7). When the initial crack is given as $z_0(x) := \zeta_0(x_1 +$

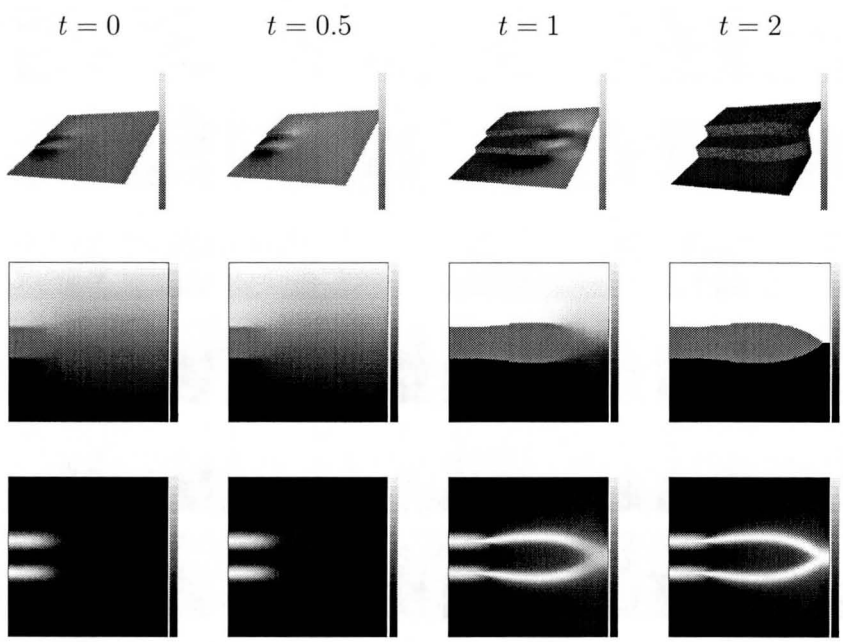

Figure 2.7: Bird's-eye views of u(top), u (middle) and z (bottom) in the temporal evolution of the cracks when initial length of cracks is 0.5.

$0.5, x_2 + 0.2) + \zeta_0(x_1 + 0.5, x_2 - 0.2)$, (Fig. 2.6 (a) and $x_0 = -0.5, y_0 = 0.2$), 2 crack merge together and grow as one and reach the opposite side (Fig. 2.7).

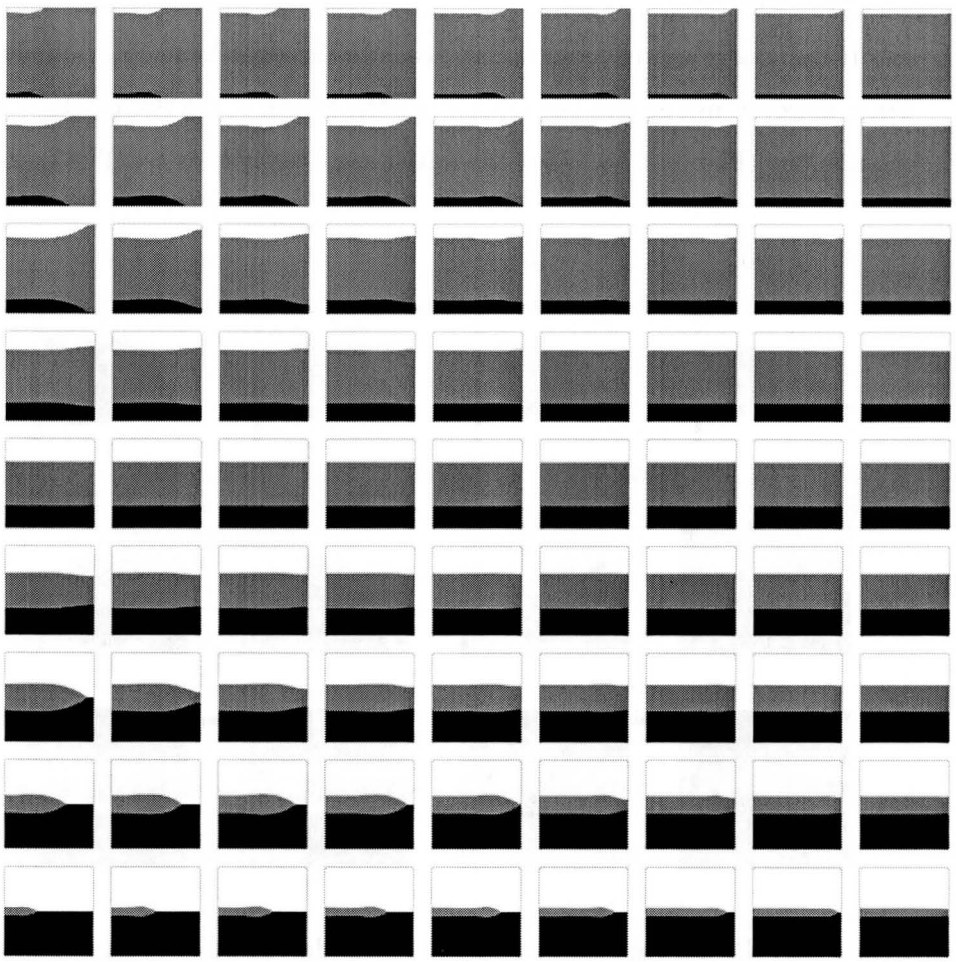

Figure 2.8: Profiles of u at $t = 2$ on various initial positions of top of the crack when 2-cracks start from the same side. Length of cracks (horizontal) v.s. width between 2 cracks (vertical).

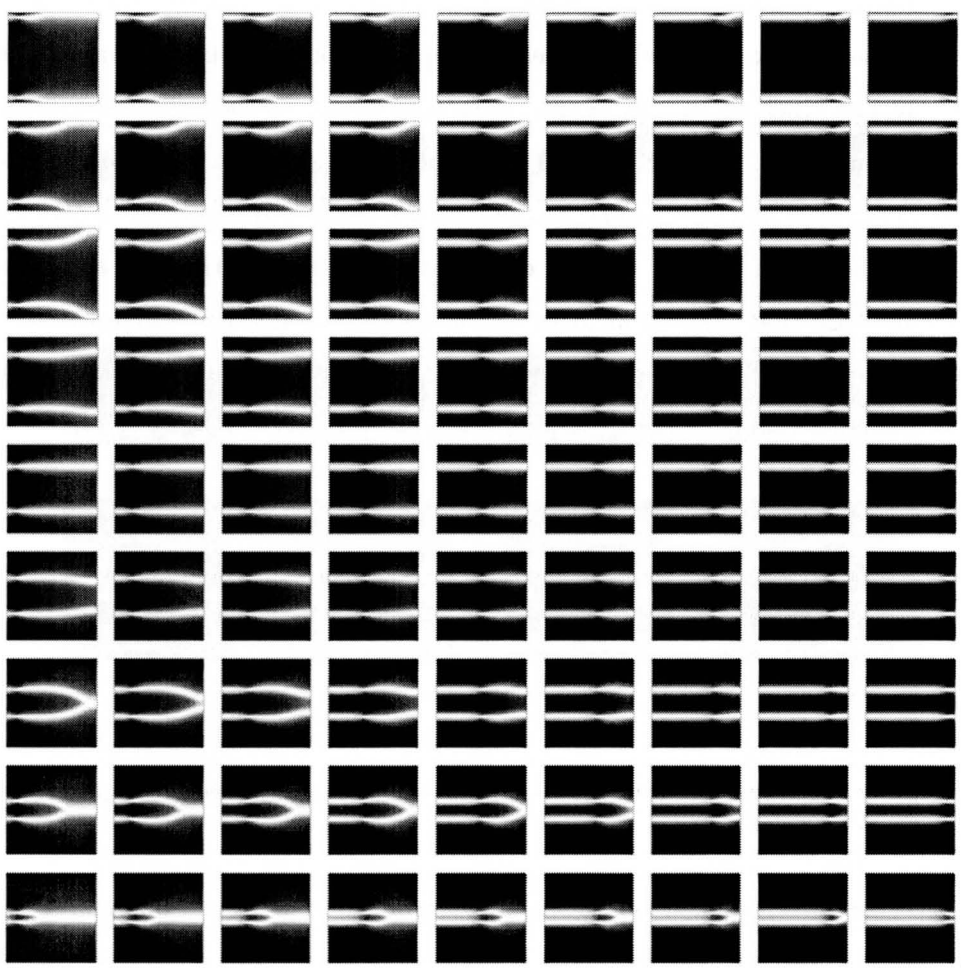

Figure 2.9: Profiles of z at $t = 2$ on various initial positions of top of the crack when 2-cracks start from the same side. Length of cracks (horizontal) v.s. width between 2 cracks (vertical).

Treating the length and the interval of the initial cracks as paramers, numerical simulations are performed. The results are categorized as follows: a) each crack separately reaches the opposite boundary, b) two cracks merge to one crack at the tip of the cracks and evolve to the opposite boundary as one crack. Fig. 2.8 and 2.9 show the profile of u and z of the numerical simulation at $t = 2$, seated as the length (horizontal) and interval (vertical) of the initial cracks. Careful examination reveal that the case a) includes the case that two cracks grow to the opposite boundary after approaching the side bundaries when the lengths of the initial cracks are sufficiently short and their interval is wide enough (Left-upper of Figure 2.8 and 2.9).

ii) Two cracks starting from opposite sides ($\gamma = 0.5$)

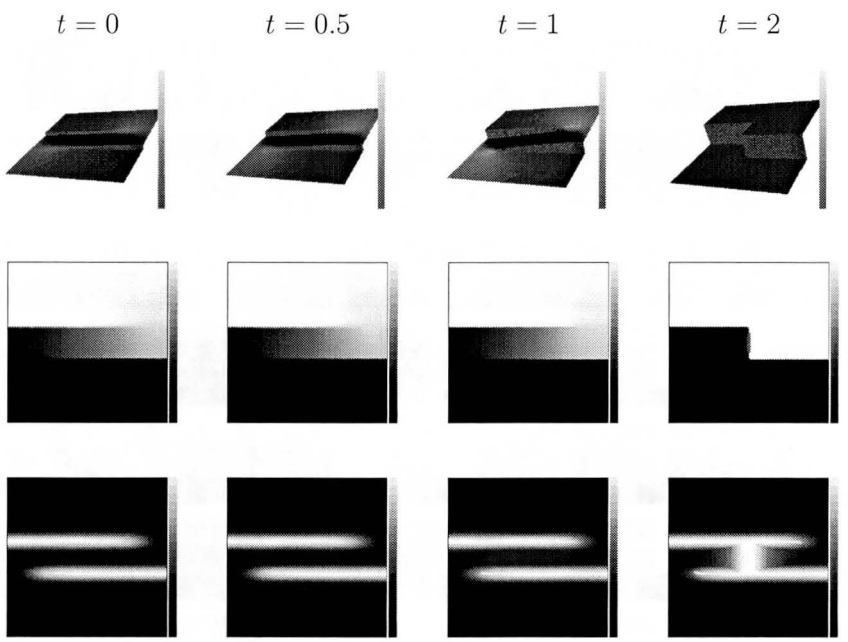

Figure 2.10: Bird's-eye views of u(top), u (middle) and z (bottom) in the temporal evolution of the cracks with initial cracks of length 1.7 .

When two cracks start from opposite sides, that is, one starts from the left-hand side boundary and another starts from the right-hand side boundary, the growth patterns are classified in three cases. Only when the initial cracks are sufficiently long, they reach the opposite boundaries (Figure 2.10). If sufficiently short cracks are initiallu set at the opposite sides, as we can easily imagine, they reach and connect to each other. But, in some middle length case, a subcrack (side-branched crack) appears .

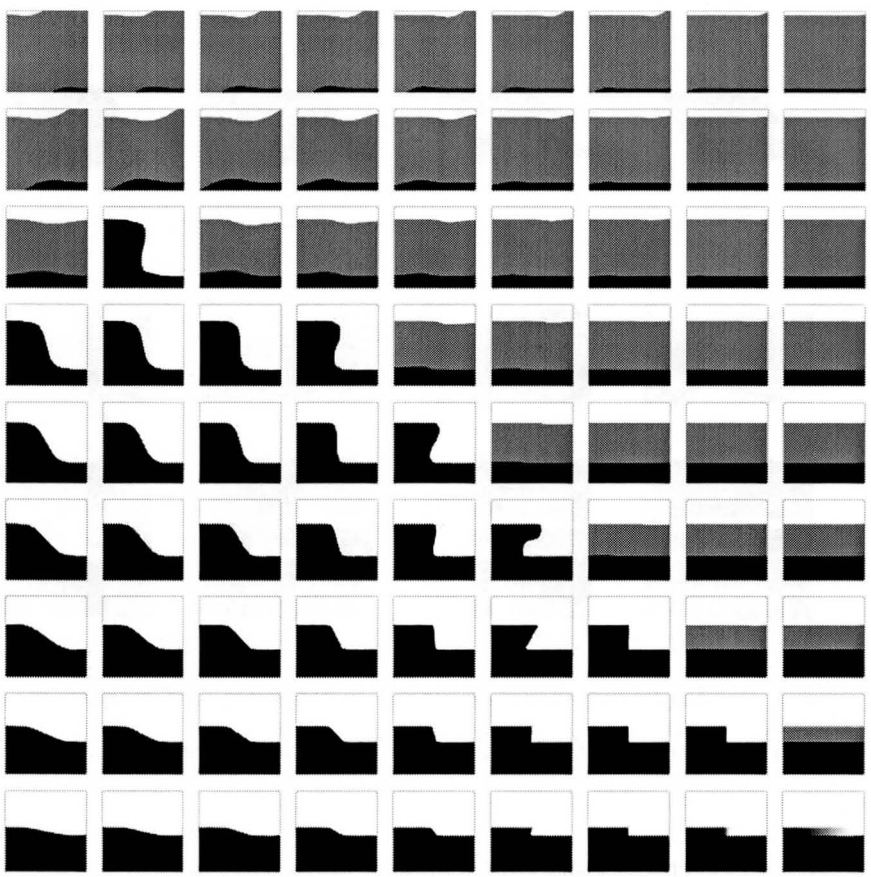

Figure 2.11: Profiles of u at $t = 2$ on various initial positions of top of the crack when 2-cracks start from the opposite sides. Length of cracks (horizontal) v.s. width between 2 cracks (vertical).

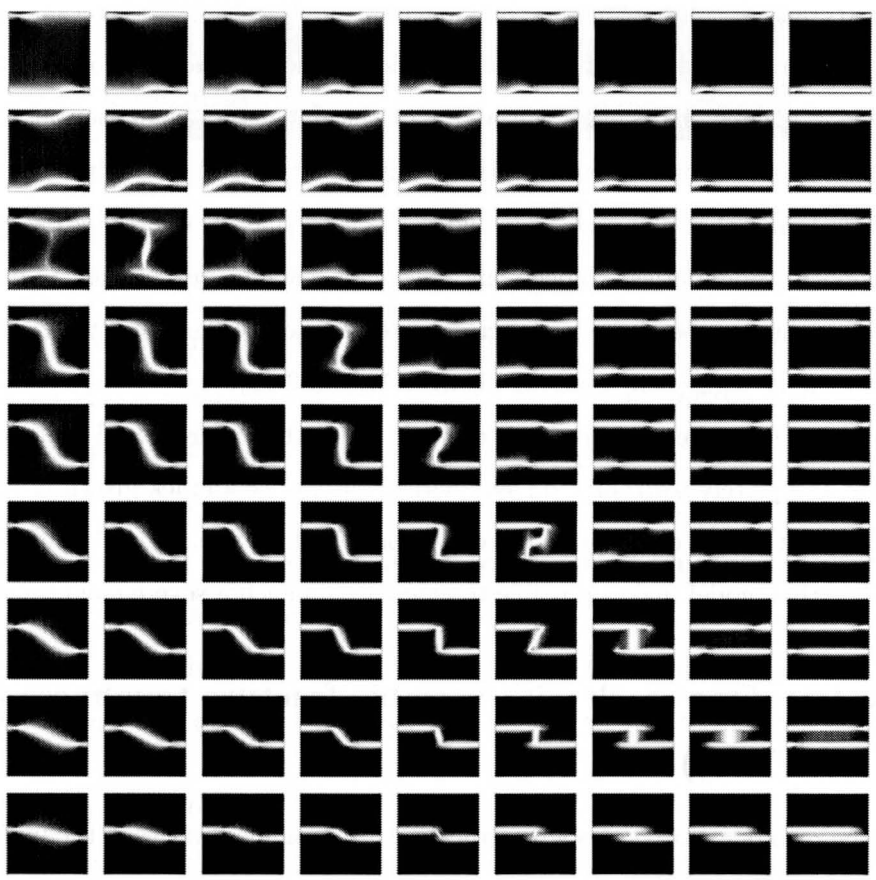

Figure 2.12: Profiles of z at $t = 2$ on various initial positions of top of the crack when 2-cracks start from the opposite sides. Length of cracks (horizontal) v.s. width between 2 cracks (vertical).

Similar to the case i), treating the length and the interval of the initial cracks as paramers of numerical simulation, it is categorized as follows: a) two cracks reach the opposite boundaries, respectively, b) two cracks connect to one crack at the tip of the cracks, c) side-branched crack appears. Fig. 2.11 and 2.12show the profile of u and z of the numerical simulation at $t = 2$, seated as the length (horizontal) and interval (vertical) of the initial cracks. It is found that the case a) includes the case that two cracks grow to the opposite boundaries, respectively, after approaching to the side bundaries when the lengths of the initial cracks are sufficiently short and their interval is wide enough (Left-upper of Figure 2.11 and 2.12).

On the real experiment it is difficult to set the experimental condition to the completely isotropic and symmetric state, once a crack growh is started from a tip of a crack, it grows only from the first one. These results show that this model makes possible to calculate on such a severe conditions.

2.4.4 One crack with variable fracture toughness ($\gamma = \gamma(x)$)

The results for two cases where the fracture toughness varies in the plane are shown. While the crack grows,on the way to the other side, the front of crack find the weak (small toughness) point and turn into there. We consider two cases where γ varies according to i) a checkerboard pattern and ii) a stripe pattern.

i) Checkerboard pattern ($\gamma(x) = 0.5(1 + 0.2\cos 10x \cdot \cos 10y)$)

A checkerboard-like distribution of the toughness shows the periodically

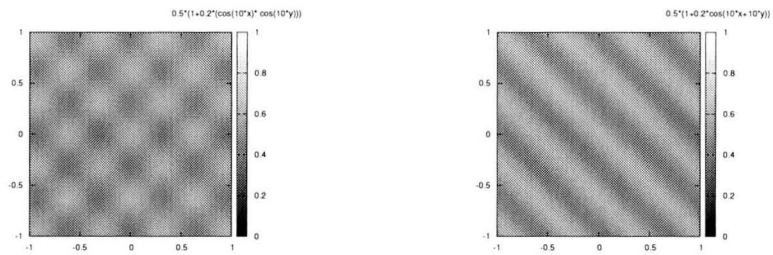

(a) (b)

Figure 2.13: Spatial profile of fructure toughness $\gamma(x)$, (a) a checkerboard pattern $\gamma(x) = 0.5(1 + 0.2\cos 10x \cos 10y))$ and (b) a stripe pattern $\gamma(x) = 0.5(1 + 0.2\cos 10(x + y))$.

fine structure that is found on many materials. When toughness $\gamma(x)$ is set as checkerboard like Figure 2.13 (a), crack grows along an elongation like zig-zag street (Figure 2.14). The crack searches the weak area and selects automatically the direction to grow.

ii) Stripe pattern ($\gamma(x) = 0.5(1 + 0.2\cos(10x + 10y))$)

Dividing the chopsticks straight is sometimes difficult when the stripe line of the wooden fiber lies slant on it. The thorny edge on the cracked surface is found. From the view point of this model, it is considered as the case that the plate has a slant stripe pattern of the toughness $\gamma(x)$ (Figure 2.13 (b)).

Figure 2.15 shows that the crack propagates to the right-hand side boundary through the weaker points of $\gamma(x)$.

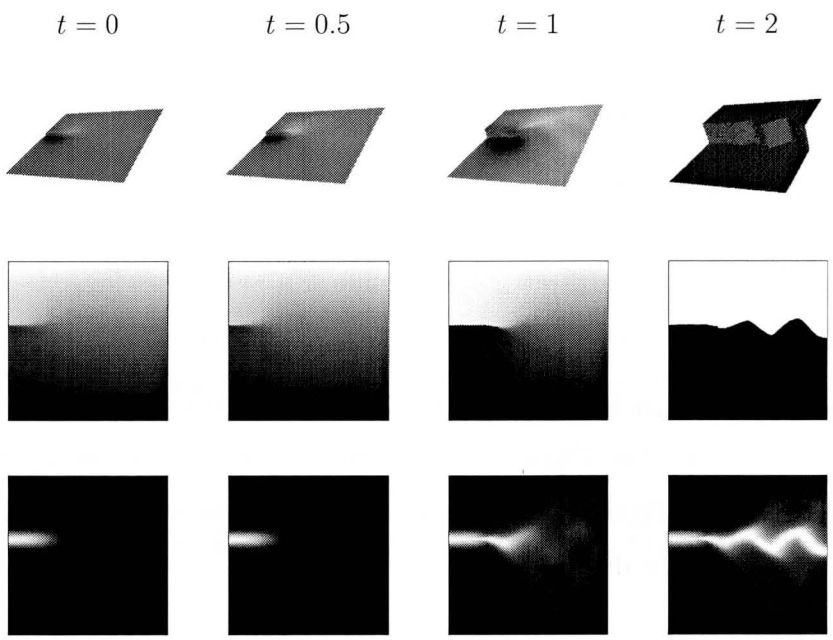

Figure 2.14: Bird's-eye views of u(top), u (middle) and z (bottom) in the temporal evolution of the cracks when $\gamma(x) = 0.5(1 + 0.2\cos 10x \cdot \cos 10y)$.

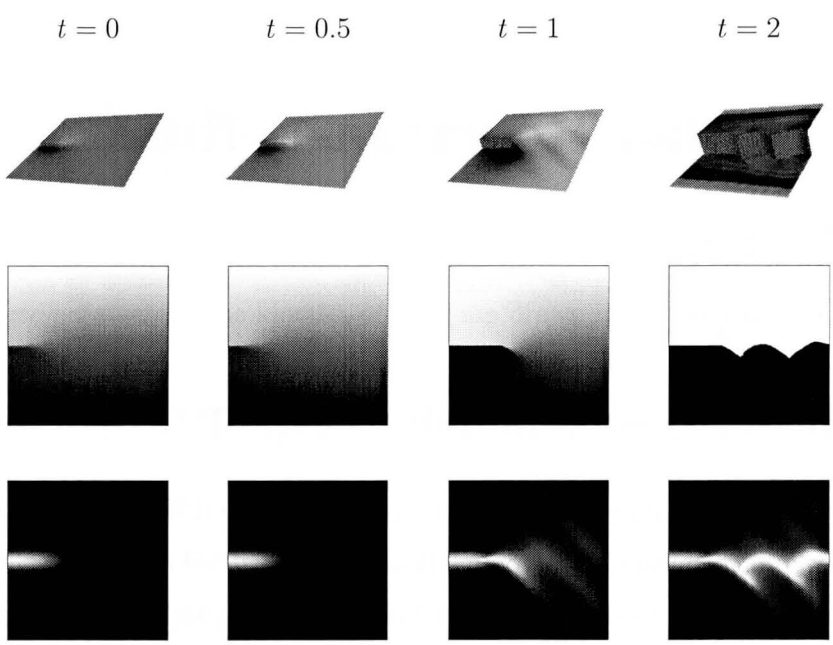

Figure 2.15: Bird's-eye views of u(top), u (middle) and z (bottom) in the temporal evolution of the cracks when $\gamma(x) = 0.5(1 + 0.2\cos 10(x + y))$.

Chapter 3

Coupled Reaction-Diffusion System

3.1 Activator-Inhibitor Type RD System

Various spatial and/or spatio-temporal patterns in diffusing media are observed in chemical physics, population dynamics, developmental biology and other fields. As an example of nonstationary or moving patterns, target and spiral waves arising in the Belousov-Zhabotinsky (BZ) reaction have been intensively investigated from the viewpoint of spatio-temporal pattern dynamics (for instance [27]).

In contrast to the BZ reaction, recently, experimental evidence of stationary or unmoving patterns has been found in a chemical system [17]. In this system, iodide (I^-) and chlorite (ClO_2^-) play the roles of an activator and its inhibitor, respectively. In order to understand theoretically the formation of such chemical patterns, a reaction-diffusion (RD) model system has

been proposed in a framework of activator-inhibitor relationship [18]. The reaction is known to be described by a five-component model consisting of three reactions, but chemically reasonable simplifications reduce it to the following two component system with u and v, which denote respectively the concentrations of I^- and ClO_2^-:

$$\begin{cases} \dfrac{\partial u}{\partial t} - d_u \Delta u = k_1 - k_2 u - \dfrac{4k_3 uv}{a+u^2} \equiv f(u,v) \\ \dfrac{\partial v}{\partial t} - d_v \Delta v = k_2 u - \dfrac{k_3 uv}{a+u^2} \equiv g(u,v), \end{cases} \tag{3.1}$$

where d_u and d_v are the effective diffusion coefficients of u and v, respectively; Δ is the Laplacian; k_1, k_2, k_3 and a are positive constants. For suitable choice of these parameters, the kinetics of (3.1) are drawn in Figure 3.1.

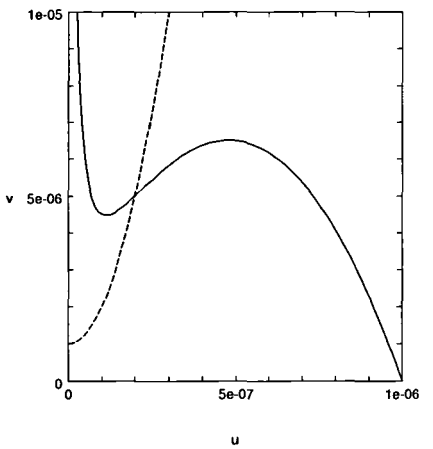

Figure 3.1: The nullclines of the nonlinealities of the Chlorite-Iodide-Malonic Acid-Starch reaction (3.1) where $k_1 = 10^{-4}, k_2 = 10^2, k_3 = 10^{-6}, a = 10^{-14}$.

Since the reaction proceeds in the gel, it is experimentarily confirmed that

I^- diffuses slowly so that the effective diffusion coefficients are estimated as $d_v/d_u = 15$. It is understood that the spatial patterns of chemicals occur due to the combination of local autocatalysis and lateral inhibition. This explanation was originally proposed by Turing to explain cell-differentiation in biology [26].

In addition to the above chemical reaction, biological patterns such as pigmentation patterns on shells and animal coat markings can be also modelled by RD systems of the type (3.1) with qualitatively similar nonlinearities ([16], [20]).

As a prototype of (3.1), the following 2-component system has been proposed in a framework of activator-inhibitor model systems:

$$\begin{cases} \dfrac{\partial u}{\partial t} &= d_u \Delta u + f(u,v) \\ \dfrac{\partial v}{\partial t} &= d_v \Delta v + \delta g(u,v) \end{cases} \tag{3.2}$$

with the Bonhoeffer-van der Pol kineteics

$$f(u,v) \equiv u(u-\alpha)(1-u) - v \quad \text{and} \quad g(u,v) \equiv u - \gamma v + \theta, \tag{3.3}$$

where u and v are two variable species respectively corresponding to the activator and its inhibitor. d_u and d_v are the diffusion rates of u and v. $1 > \alpha > 0$, $\gamma > 0$ and θ are constants. δ is the time constant related to the kinetics. For suitable choice of γ and θ such that nonlinearities of f and g are given as in Figure 3.2, one finds the kinetics (3.3) are qualitatively similar to the ones in (3.1) where (3.2) has a unique spatially constant equilibrium solution, say $(\tilde{u}, \tilde{v})$.

In addition to the above situation, if the activator diffuses more slowly

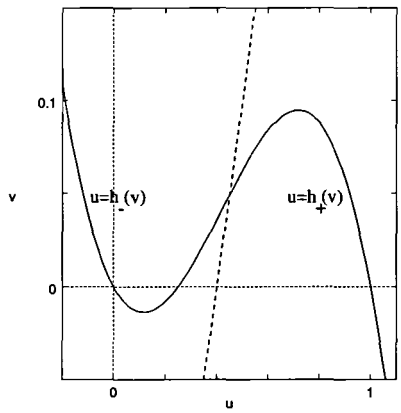

Figure 3.2: The nullclines of f and g in (3.3) where $\alpha = 0.25, \gamma = 1, \theta = -0.4$.

than the inhibitor does ($d_u < d_v$), the system falls into the framework of Turing's diffusive instability so that spatially inhomogeneous stationary patterns with stripe or hexagonal structures appear in higher dimensions [21].

Under this framework, we assume that the activator diffuses much more slowly than the inhibitor does ($d_u << d_v$). With suitable transformations $\varepsilon = \sqrt{d_u}$, $\tau = \delta/\sqrt{d_u}$ and $d = d_v/\delta$, it is convenient to rewrite (3.2) as

$$\begin{cases} \tau \dfrac{\partial u}{\partial t} &= \varepsilon \Delta u + \dfrac{1}{\varepsilon} f(u,v) \\ \dfrac{\partial v}{\partial t} &= d\Delta v + g(u,v), \end{cases} \tag{3.4}$$

where we assume d is of the order $O(1)$ with sufficiently small ε. The system (3.4) can be interpreted as follows: If $\tau = O(1/\varepsilon)$, then u and v react to the same degree, but u diffuses much slower than v does; if $\tau = O(1)$, u reacts faster than v does, and u diffuses slower than v does. If $\tau = O(\varepsilon)$, u reacts much faster than v does, but u and v diffuse to the same degree.

We consider (3.4) with the case when $\tau = O(1)$ in a bounded domain Ω

with the zero-flux boundary conditions

$$\frac{\partial u}{\partial n} = 0 = \frac{\partial v}{\partial n} \tag{3.5}$$

on the boundary $\partial\Omega$, where n is the outward normal vector on $\partial\Omega$.

Since ε is sufficiently small, (3.4) can be approximated by $u_t \approx (1/\varepsilon)f(u, v(x, 0))$ in a short time so that almost all of u takes either $h_+(v(x, 0))$ or $h_-(v(x, 0))$ in Ω, where $u = h_\pm(v)$ are two stable branches of $f(u, v) = 0$, as seen in Figure 3.2. This indicates that the u-component approximately is separated into two different states which are connected by internal layers in a way that Ω consists of three parts Ω_+, Ω_- and Ω_0 where $\Omega_\pm = \{(x, y) \in \Omega | u \approx h_\pm(v)\}$, and Ω_0 is the layer region between $\Omega_\pm$. Figures 3.3 and 3.4 show a time evolution of a 2 dimensional solution of (3.4), (3.5). It clearly shows that there appear internal layers which distinginshes into two different states in the u-component, and that the subsequent time evolution of patterns is described by the dynamics of these layers.

From the layer dynamics viewpoint, theoretical studies of (3.4), (3.5) have recently progressed [25]. Especially, the existence and stability of nonconstant equilibrium solutions with internal layers (we call them simply *layer-equilibrium solutions*) of the 1 dimensional problems of (3.4), (3.5) can be discussed almost completely by using singular limit analysis as $\varepsilon \downarrow 0$ ([19], [23]) . It is known that these solutions are stable for large τ, while, when τ decreases, these become unstable through Hopf bifurcation and there appear spatio-temporal periodic solutions with oscillating layers (Figure 3.5)[24].

For this reason, one finds that the system (3.4) with (3.5) is one of *pattern generators.*

Chemical and biological systems may generally communicate by exchange

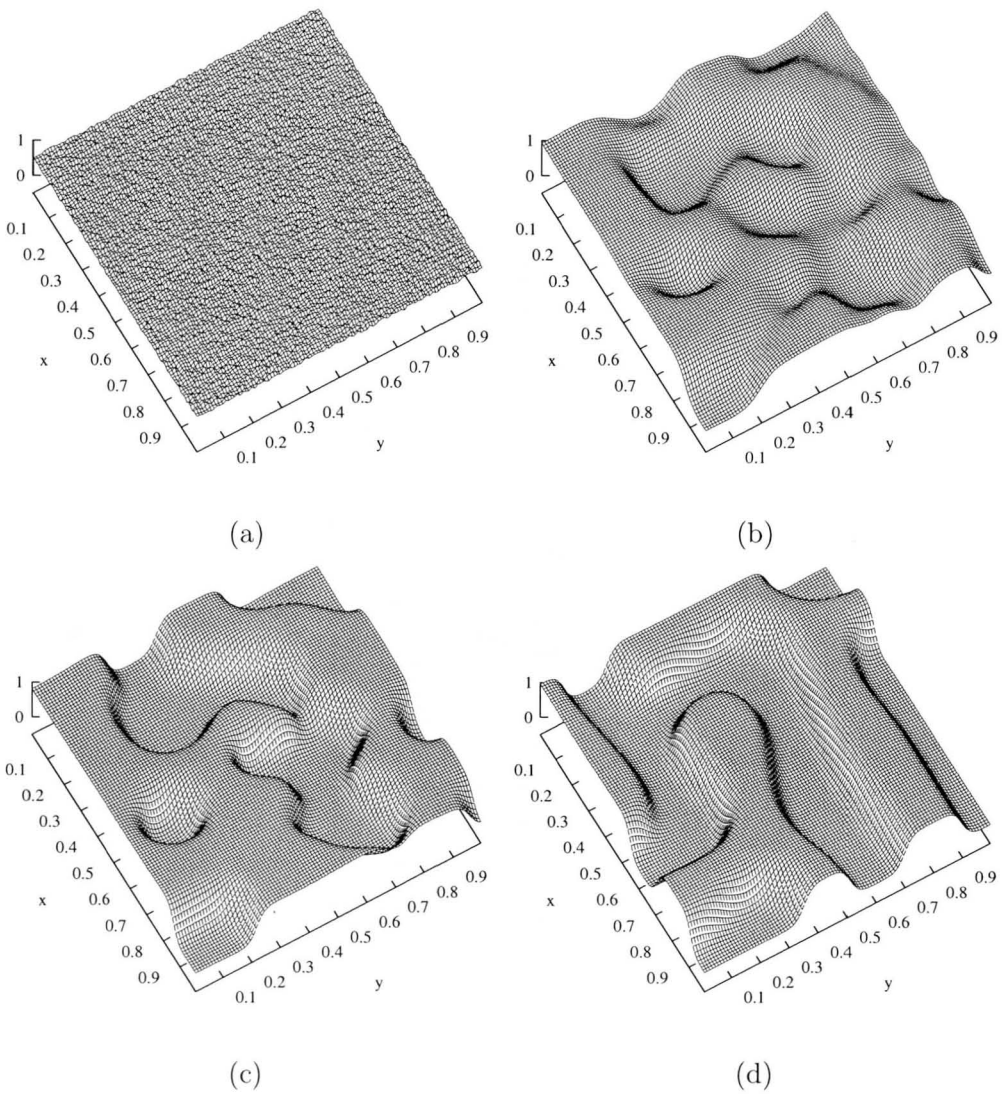

Figure 3.3: Spatial profile of the u-component of the 2 dimensional system of (3.4) when $\tau = 1.0, \varepsilon = 0.01, d = 0.1, \alpha = 0.5, \gamma = 3, \theta = -0.5, L = 1$. (a) Time = 0 (random initial state). (b) Time = 0.3. (c) Time = 0.5. (d) Time = 10.0.

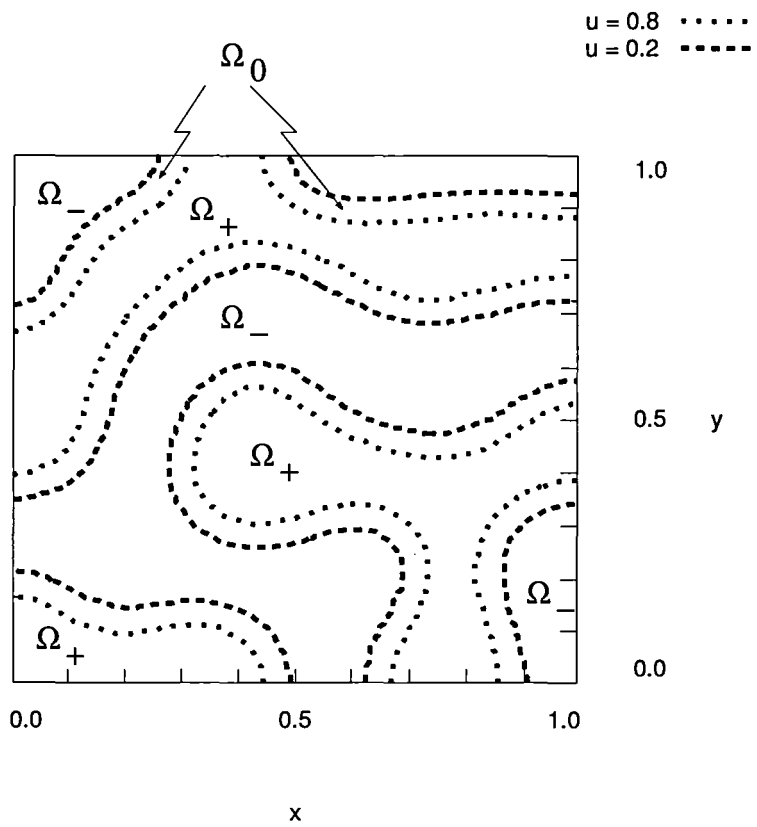

Figure 3.4: Spatial profile of the u-component of the 2 dimensional system of (3.4) when $\tau = 1.0, \varepsilon = 0.01, d = 0.1, \alpha = 0.5, \gamma = 3, \theta = -0.5, L = 1$. Contour plot at $u = 0.5$ when time $= 10.0$. The interval $\Omega = (0, L) \times (0, L)$ is divided into three parts: Ω_+, Ω_-, and Ω_0.

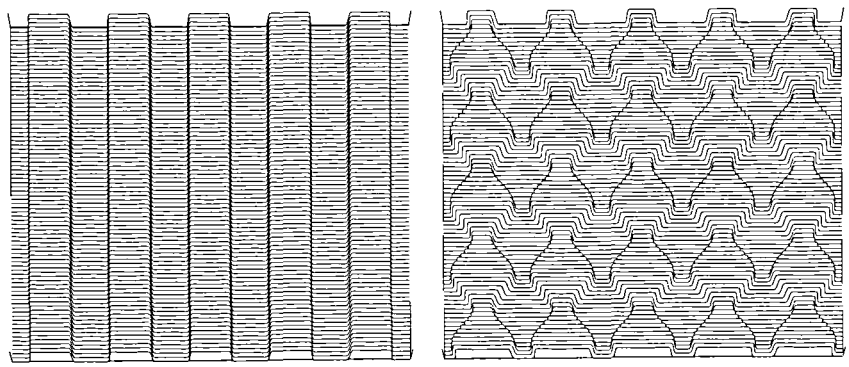

(a) (b)

Figure 3.5: (a) The dynamics of the 10-layer equilibrium solution of u of (3.4) when $\tau = 0.1, \varepsilon = 0.01, d = 4, \alpha = 0.25, \gamma = 1, \theta = -0.4, L = 10$. (b) The dynamics of the 10-layer oscillatory solution of u of (3.4) when $\tau = 0.08, \varepsilon = 0.01, d = 4, \alpha = 0.25, \gamma = 1, \theta = -0.4, L = 10$.

of species involved in the systems through a membrane. This suggests studying the membrane coupling by diffusive transport between two activator-inhibitor systems. Along this line, Winston et.al [28] have recently reported the dynamical behaviour arising from the diffusive membrane coupling of spiral patterns in the BZ reaction reagent, and also, using two coupled model equations of (3.4) with $d = 0$, they numerically demonstrate that the coupling of two spiral waves gives rise to dynamical patterns which never appear in decoupled systems.

Motivated by the above, we are interested in the coupling of stable patterns arising in decoupled systems (3.4) with (3.5). The essential difference from Winston et.al is that the diffusivity of the inhibitor is very large com-

pared with that of the activator.

In order to study the diffusive membrane coupling of patterns in the decoupled systems, we propose the following RD equations with the coupling coefficient $k > 0$:

$$\begin{cases} \tau \dfrac{\partial u_1}{\partial t} &= \varepsilon \Delta u_1 + \dfrac{1}{\varepsilon} f(u_1, v_1) \\ \dfrac{\partial v_1}{\partial t} &= d\Delta v_1 + g(u_1, v_1) + k(v_2 - v_1) \\ \tau \dfrac{\partial u_2}{\partial t} &= \varepsilon \Delta u_2 + \dfrac{1}{\varepsilon} f(u_2, v_2) \\ \dfrac{\partial v_2}{\partial t} &= d\Delta v_2 + g(u_2, v_2) + k(v_1 - v_2) \end{cases} \quad t > 0, (x, y) \in \Omega, \tag{3.6}$$

with the boundary conditions

$$\frac{\partial u_i}{\partial n} = 0 = \frac{\partial v_i}{\partial n} \quad (i = 1, 2) \quad t > 0, (x, y) \in \partial\Omega, \tag{3.7}$$

where Ω is a bounded domain with boundary $\partial\Omega$. (3.6) indicates that the direct coupling only proceeds between v_1 and v_2.

Since (3.4), (3.5) is the decoupled problem of (3.6), (3.7), we note that $(u_1, v_1; u_2, v_2) = (u, v; u, v)$ is a *trivial* solution of (3.6), (3.7) for any $k > 0$, if (u, v) is a solution of (3.4), (3.5).

We numerically demonstrate the effect of the coupling parameter k on the stability of a trivial 2 dimensional equilibrium solution $(\tilde{u}(x, y), \tilde{v}(x, y); \tilde{u}(x, y), \tilde{v}(x, y))$ of (3.6), (3.7). Here, $(\tilde{u}(x, y), \tilde{v}(x, y))$ is the stable equilibrium solution of (3.4), (3.5) which was obtained in Figure 3.3 and Figure 3.4. We take the trivial equilibrium solution with small disturbances as an initial function and compute (3.6), (3.7) when k is varied. For $k = 0.5$, the trivial equilibrium solution is stable, even if the disturbances are not small. However, for

$k = 1$, 2, and 5, it is no longer stable but the solution tends to a nontrivial 2 dimensional equilibrium solution $(\tilde{u}_1(x,y), \tilde{v}_1(x,y); \tilde{u}_2(x,y), \tilde{v}_2(x,y))$, as in Figure 3.6. These numerical results indicate two features: (i) Stability of the trivial equilibrium solution clearly depends on the value of k; (ii)The shapes of $\tilde{\Omega}_{+i} = \{(x,y) \in \Omega | \tilde{u}_i \approx h_+(\tilde{v}_i)\}(i = 1,2)$, which is called the excited domain of u_i, are shifted in such a way that the overlapped region of $\tilde{\Omega}_{+1} \cap \tilde{\Omega}_{+2}$ decreases when k increases. In fact, when $k = 5$, $\tilde{u}_1(x,y)$ and $\tilde{u}_2(x,y)$ are separated almost completely as in Figure 3.6 (d). For the 1 dimensional problem of (3.6), (3.7), we find the k-dependency of the solution more qualitatively. For the interval $I = (0, L)$ with arbitrarily fixed $L > 0$, the problem is

$$\begin{cases} \tau \dfrac{\partial u_1}{\partial t} &= \varepsilon \dfrac{\partial^2 u_1}{\partial x^2} + \dfrac{1}{\varepsilon} f(u_1, v_1) \\ \dfrac{\partial v_1}{\partial t} &= d \dfrac{\partial^2 v_1}{\partial x^2} + g(u_1, v_1) + k(v_2 - v_1) \\ \tau \dfrac{\partial u_2}{\partial t} &= \varepsilon \dfrac{\partial^2 u_2}{\partial x^2} + \dfrac{1}{\varepsilon} f(u_2, v_2) \\ \dfrac{\partial v_2}{\partial t} &= d \dfrac{\partial^2 v_2}{\partial x^2} + g(u_2, v_2) + k(v_1 - v_2) \end{cases} \quad t > 0, x \in I \qquad (3.8)$$

with the boundary conditions

$$\frac{\partial u_i}{\partial x} = 0 = \frac{\partial v_i}{\partial x} \quad (i = 1,2) \quad t > 0, x = 0, L. \qquad (3.9)$$

Obviously, the decoupled version of (3.8), (3.9) is

$$\begin{cases} \tau \dfrac{\partial u}{\partial t} &= \varepsilon \dfrac{\partial^2 u}{\partial x^2} + \dfrac{1}{\varepsilon} f(u, v) \\ \dfrac{\partial v}{\partial t} &= d \dfrac{\partial^2 v}{\partial x^2} + g(u, v) \end{cases} \quad t > 0, x \in I \qquad (3.10)$$

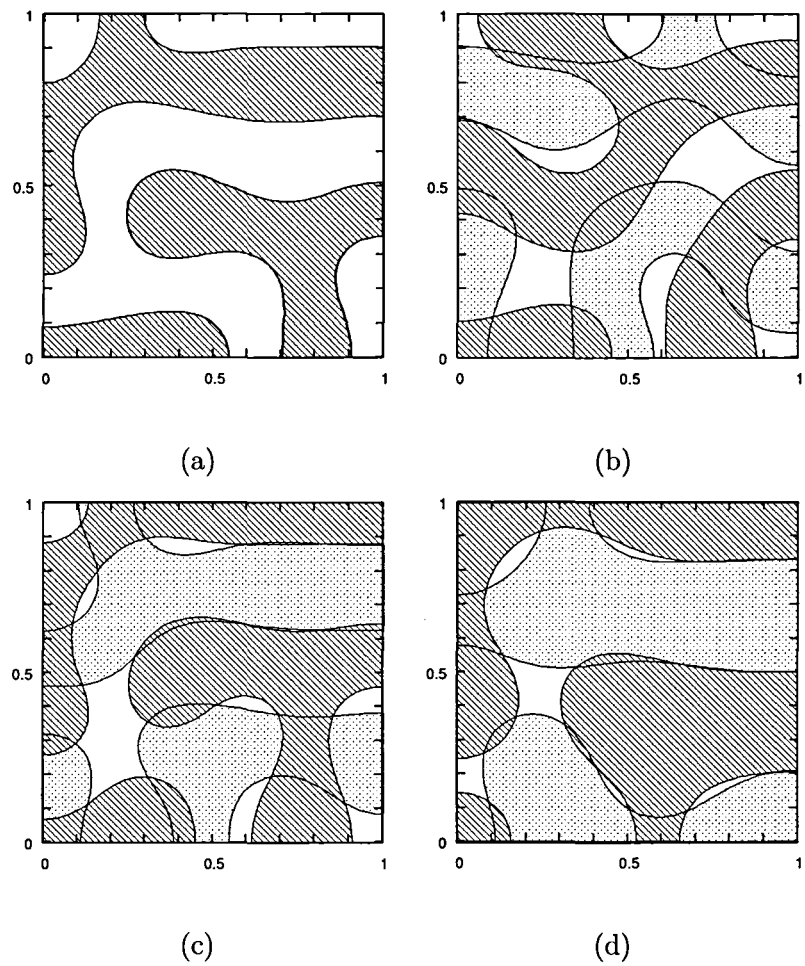

Figure 3.6: Contour plot of u_1 and u_2 of 2 dimensional coupled RD system at $u_i = 0.5$ $(i = 1, 2)$ for some coupling strength (a)$k = 0.5$, (b) 1, (c) 2, (d) 5. The Ω_{+1} domain is shaded with straight lines, and the Ω_{+2} domain is shaded with dots. When $k = 0.5$, the decoupled pattern is still stable, however, when $k = 1, 2$ patterns on each RD system move differentely. Moreover, when $k = 5$, the overlapped region between two RD system is almost extinct.

with the boundary conditions

$$\frac{\partial u}{\partial x} = 0 = \frac{\partial v}{\partial x} \quad t > 0, x = 0, L. \tag{3.11}$$

To study the stability of the trivial equilibrium solutions, we take the trivial equilibrium solution with small disturbances as initial functions. In a similar way to $\Omega_{\pm i}$ in 2 dimension , we use the symbols $I_{\pm i}$ for the excited domain of $u_i(x,t)$, $(i = 1,2)$ to explain the interaction of $(u_1(x,t), v_1(x,t))$ and $(u_2(x,t), v_2(x,t))$. It is obvious that $I_{\pm 1} = I_{\pm 2}$ for the trivial solution. We found the following: For small k (weak coupling), the trivial solution is stable, as is expected, while for large k (strong coupling), it becomes unstable and there exist stable nontrivial equilibrium solutions for which I_{+1} and I_{+2} (respectively I_{-1} and I_{-2}) locate alternately in such a way that all of the layers in $u_1(x,t)$ (respectively $u_2(x,t)$) shift to the right or left (respectively left or right) direction, as in Figures 3.7 and 3.8. We may call such pattern "*alternated*" or "*toothed wheel-like*". In a 1-layer system, there appear anti-directionally shifted patterns, however, we similarly call them the alternated patterns.

It is also of interest to consider the stability of the trivial periodic solutions $(u^p(x,t), v^p(x,t);\ u^p(x,t), v^p(x,t))$, assuming that $(u^p(x,t), v^p(x,t))$ is a stable periodic solution of (3.10), (3.11). The trivial periodic solution is stable for small k, while it becomes unstable for large k, and there exist stable nontrivial equilibrium solutions with alternated patterns, which is the same one as was shown above. Furthermore, even if the initial function of $(u_1, v_1; u_2, v_2)$ takes $(u^p(x,0), v^p(x,0); u^p(x,\tau), v^p(x,\tau))$ for any $\tau \in (0,T)$ with the time period T, it is numerically confirmed that the similar dynamical behaviour occurs.

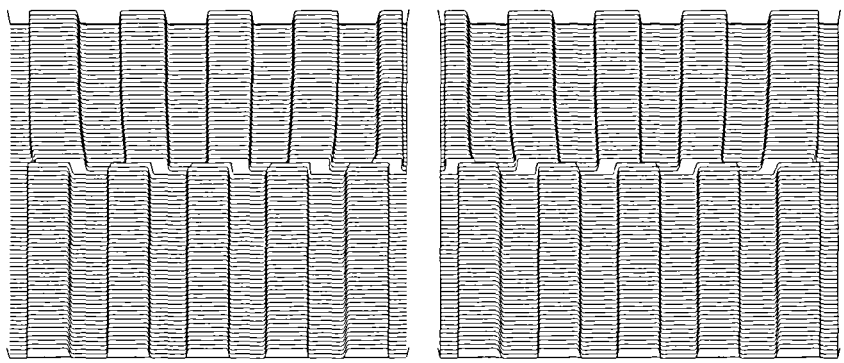

u_1 u_2

Figure 3.7: The dynamics of u of the solution of (3.8), (3.9) where $\tau = 0.2, \varepsilon = 0.01, d = 4.0, \alpha = 0.25, \gamma = 1, \theta = -0.4, L = 10$ and $k(t) = 0.0(0 < t < 200),\ 20.0(200 < t)$

These numerical observations indicate that when k is large, regardless to the trivial solution being either stationary or periodic, it becomes unstable in the coupled system, and there exist stable nontrivial equilibrium solutions which exhibit an "*alternated pattern*" . The purpose here is to understand such behavior from the viewpoint of bifurcation.

In Section 3.2, we derive the coupled system (3.8), (3.9) from two systems with a diffusive membrane boundary condition. In Section 3.3, we numerically investigate the global structure of a 1-layer equilibrium and periodic solutions of (3.8), (3.9) as k is varied. In Section 3.4, we study the stability of the trivial 1-layer equilibrium solutions of (3.8), (3.9), by using the spectral analysis in the limit $\varepsilon \downarrow 0$. Finally, a few remarks are given in Section 3.5.

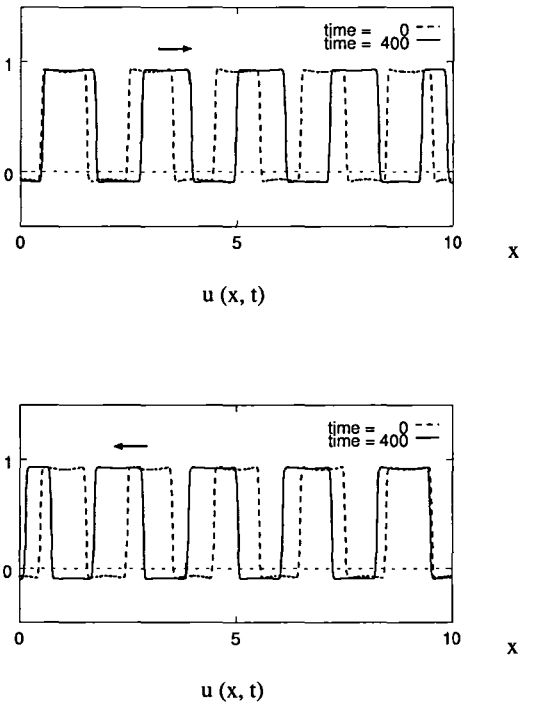

Figure 3.8: Spatial profiles of u_1 and u_2 in Figure 3.7 at $t = 0$ and $t = 400$. An alternated pattern, in which the layers in u_1 shift to the right and those in u_2 shift to the left, appears in the coupled system.

3.2 Settings of the Coupled RD Systems

In order to derive the coupled system (3.8) with (3.9) in a 2 dimensional domain Ω, we present two RD systems of the form (3.4) for (u_i, v_i) in the 3

dimensional domains $\tilde{\Omega}_i$ $(i = 1, 2)$

$$\begin{cases} \tau \dfrac{\partial u_i}{\partial t} &= \varepsilon \triangle u_i + \dfrac{1}{\varepsilon} f(u_i, v_i) \\ \dfrac{\partial v_i}{\partial t} &= d \triangle v_i + g(u_i, v_i), \end{cases} \quad t > 0, (x, y, z) \in \tilde{\Omega}_i \ (i = 1, 2), \tag{3.12}$$

where $\tilde{\Omega}_i$ $(i = 1, 2)$ are given by

$$\tilde{\Omega}_1 = \{(x, y, z) \in \mathbf{R}^3 | (x, y) \in \Omega, 0 < z < l\}$$

$$\tilde{\Omega}_2 = \{(x, y, z) \in \mathbf{R}^3 | (x, y) \in \Omega, -l < z < 0\}$$

with the base rectangular region $\Omega = (0, L) \times (0, L)$ and the thickness l. The symbol $\Delta = \partial^2/\partial x^2 + \partial^2/\partial y^2 + \partial^2/\partial z^2$ stands for the 3-dimensional Laplace operator. On the common boundary we impose the following conditions.

$$\begin{cases} -\varepsilon \dfrac{\partial u_1}{\partial z} = -\varepsilon \dfrac{\partial u_2}{\partial z} = k_u (u_2 - u_1) \\ -d \dfrac{\partial v_1}{\partial z} = -d \dfrac{\partial v_2}{\partial z} = k_v (v_2 - v_1), \end{cases} \tag{3.13}$$

$$t > 0, (x, y, z) \in \tilde{\Omega}_m = \{(x, y, z) \in \mathbf{R}^3 | (x, y) \in \Omega, z = 0\},$$

where k_u and k_v are the transport rates of u_i and $v_i (i = 1, 2)$ through $\tilde{\Omega}_m$. The conditions (3.13) imply that the plane $\tilde{\Omega}_m$ is a *"diffusive"* membrane (Figure 3.9). Other boundary conditions at $\partial\tilde{\Omega} \backslash \tilde{\Omega}_m$ with $\tilde{\Omega} = \tilde{\Omega}_1 \cup \tilde{\Omega}_2 \cup \tilde{\Omega}_m$ are

$$\frac{\partial u_i}{\partial n} = 0 = \frac{\partial v_i}{\partial n}, \quad (i = 1, 2), \tag{3.14}$$

where n is the outward normal vector on the boundary $\partial\tilde{\Omega}$.

In order to understand the coupling between (u_1, v_1) and (u_2, v_2) in (3.12) through the boundary conditions (3.13), we assume that l is sufficiently small

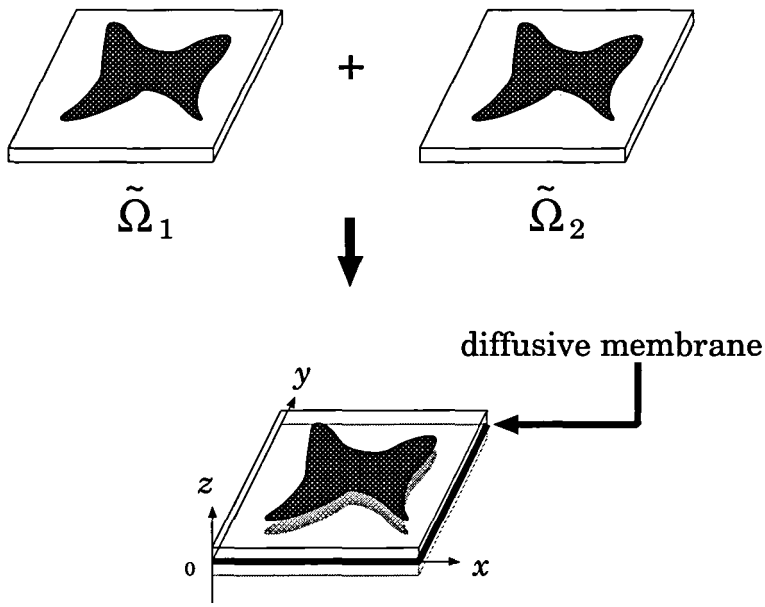

Figure 3.9: The coupled system consisting of two box domain $\tilde{\Omega}_1$ and $\tilde{\Omega}_2$ which interact through the *"diffusive"* membrane between them.

and then reduce the 3 dimensional problem (3.12) - (3.14) to the 2 dimensional one by taking the limit $l \downarrow 0$. Taking the spatial average of u_1 with z-direction for the first equation of (3.12), we have

$$\frac{\tau}{l}\frac{\partial}{\partial t}\int_0^l u_1 dz = \frac{1}{l}\int_0^l \varepsilon \Delta u_1 dz + \frac{1}{\varepsilon l}\int_0^l f(u_1, v_1) dz. \tag{3.15}$$

By using (3.13) and (3.14), the diffusion term of u_1 to the z-direction is written as

$$\frac{1}{l}\int_0^l \varepsilon \frac{\partial^2 u_1}{\partial z^2} dz = \frac{1}{l}\varepsilon \left[\frac{\partial u_1}{\partial z}\right]_{z=0}^{l} = \frac{1}{l}k_u(u_2 - u_1).$$

Similar expressions are obtained for u_2, v_1, and v_2.

Suppose that k_u and k_v are very small in the sense that $k_u = k_{u0}l^\beta$ and $k_v = k_{v0}l^\beta$ with some constant $\beta > 0$. Taking the limit $l \downarrow 0$, one could expect that (u_i, v_i) $(i = 1, 2)$ are nearly uniform in the direction of the z-axis, and thus, we formally derive a 2 dimensional system for $(u_1(x, y, t), v_1(x, y, t); u_2(x, y, t), v_2(x, y, t))$ from (3.15). It turns out that its form depends on the value of β as follows:

(i) $(0 < \beta < 1)$

For this case, $\lim_{l\to 0}(k_u/l) = \infty = \lim_{l\to 0}(k_v/l)$; that is, the transport rates become infinity, so that $u_1 = u_2 = u$ and $v_1 = v_2 = v$ hold for large time. It implies the diffusive homogenization between (u_1, v_1) and (u_2, v_2). Then, the limiting system of (3.12), (3.13) as $l \downarrow 0$ is

$$\begin{cases} \tau\dfrac{\partial u}{\partial t} &= \varepsilon\Delta u + \dfrac{1}{\varepsilon}f(u,v) \\ \dfrac{\partial v}{\partial t} &= d\Delta v + g(u,v) \end{cases} \quad t > 0, (x,y) \in \Omega,$$

where $\Delta = \partial^2/\partial x^2 + \partial^2/\partial y^2$.

(ii) $(\beta = 1)$

For this case, $\lim_{l\to 0}(k_u/l) = k_{u0}$ and $\lim_{l\to 0}(k_v/l) = k_{v0}$ so that the limiting system is

$$\begin{cases} \tau\dfrac{\partial u_1}{\partial t} &= \varepsilon\Delta u_1 + \dfrac{1}{\varepsilon}f(u_1,v_1) + k_{u0}(u_2 - u_1) \\ \dfrac{\partial v_1}{\partial t} &= d\Delta v_1 + g(u_1,v_1) + k_{v0}(v_2 - v_1) \\ \tau\dfrac{\partial u_2}{\partial t} &= \varepsilon\Delta u_2 + \dfrac{1}{\varepsilon}f(u_2,v_2) + k_{u0}(u_1 - u_2) \\ \dfrac{\partial v_2}{\partial t} &= d\Delta v_2 + g(u_2,v_2) + k_{v0}(v_1 - v_2) \end{cases} \quad t > 0, (x,y) \in \Omega, \quad (3.16)$$

which is a truly coupled system for (u_i, v_i) $(i = 1, 2)$.

(iii) $(\beta > 1)$

For this case, $\lim_{l\to 0}(k_u/l) = 0 = \lim_{l\to 0}(k_v/l)$; that is, there is no transportation between Ω_1 and Ω_2 so that the limiting system is

$$\begin{cases} \tau\dfrac{\partial u_i}{\partial t} &= \varepsilon\Delta u_i + \dfrac{1}{\varepsilon}f(u_i, v_i) \\ \dfrac{\partial v_i}{\partial t} &= d\Delta v_i + g(u_i, v_i) \end{cases} \quad t > 0, (x, y) \in \Omega, (i = 1, 2), \tag{3.17}$$

for which (u_1, v_1) and (u_2, v_2) are completely isolated.

In this paper, we concentrate our study on the 1 dimensional system of (3.16) assuming that

$$\begin{cases} k_{u0} &= 0 \\ k_{v0} &= k, \end{cases} \tag{3.18}$$

which implies that the activator can scarcely pass through the diffusive membrane because the activator diffuses much more slowly than inhibitor does, as $k_{u0}/k_{v0} \sim O(\varepsilon)$.

Then the resulting system is

$$\begin{cases} \tau\dfrac{\partial u_1}{\partial t} &= \varepsilon\dfrac{\partial^2 u_1}{\partial x^2} + \dfrac{1}{\varepsilon}f(u_1, v_1) \\ \dfrac{\partial v_1}{\partial t} &= d\dfrac{\partial^2 v_1}{\partial x^2} + g(u_1, v_1) + k(v_2 - v_1) \\ \tau\dfrac{\partial u_2}{\partial t} &= \varepsilon\dfrac{\partial^2 u_2}{\partial x^2} + \dfrac{1}{\varepsilon}f(u_2, v_2) \\ \dfrac{\partial v_2}{\partial t} &= d\dfrac{\partial^2 v_2}{\partial x^2} + g(u_2, v_2) + k(v_1 - v_2) \end{cases} \quad t > 0, x \in I = (0, L) \tag{3.19}$$

with the boundary conditions

$$\frac{\partial u_i}{\partial x} = 0 = \frac{\partial v_i}{\partial x} \quad (i = 1, 2), t > 0, x = 0, L, \tag{3.20}$$

which are the same ones as (3.8), (3.9).

Our purpose is to study the stability of trivial equilibrium solutions for the problem (3.19), (3.20) when the coupling parameter k is globally varied and to investigate what kind of patterns develop when the trivial solution becomes unstable.

3.3 Emergence of new staionary patterns through strong coupling

3.3.1 1-layer case

In this section, taking $L = 1$, we numerically study the coupling of 1-layer equilibria or periodic solutions of (3.8), (3.9). Before doing it, we note that if $(\tilde{u}^*(x), \tilde{v}^*(x))$ is the equilibrium solution of (3.10), (3.11), then so is the reflected image at $x = 1/2$, $({}^*\tilde{u}(x), {}^*\tilde{v}(x)) = (\tilde{u}^*(1-x), \tilde{v}^*(1-x))$.

We first remark that there is a critical value τ^* such that the 1-layer equilibrium solutions of (3.8) with (3.9) are stable in the decoupled system ($i.e., k = 0$) when $\tau > \tau^*$; however, they become unstable through the Hopf bifuraction, and the stable 1-layer periodic solutions exist when $\tau < \tau^*$ [24]. Therefore the coupling interactions of 1-layer patterns are classified into the following four cases.

(I) Coupling of $(\tilde{u}^*(x), \tilde{v}^*(x))$ and $(\tilde{u}^*(x), \tilde{v}^*(x))$

We consider the case $(u_1, v_1) = (u_2, v_2) = (\tilde{u}^*(x), \tilde{v}^*(x))$ which is stable in the decoupled system (3.10), (3.11) (Figure 3.3.1 (a)).

Our interest is the stability of the trivial solution $(\tilde{u}^*(x), \tilde{v}^*(x))$ of (3.8),

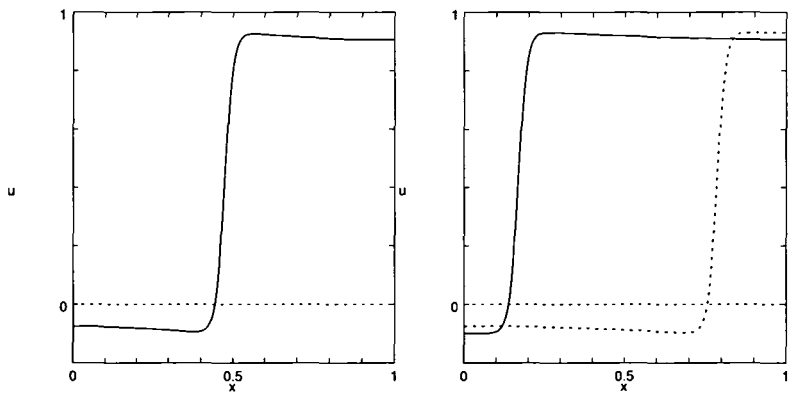

(a) (b)

Figure 3.10: The spatial profiles of u_1 (solid line) and u_2 (hashed line) of the nontrivial equilibrium solution of the 1-layer coupled RD system, (3.8), (3.9), where $\tau = 0.2, \varepsilon = 0.01, d = 4, \alpha = 0.25, \gamma = 1, \theta = -0.4, L = 1$. (a) When $k = 5$, trivial equilibrium solution is stable. (b) When $k = 20$, trivial equilibrium solution becomes unstable and the nontrivial equilibrium solution becomes stable.

(3.9) when the coupling parameter k is globally varied. The result is as follows: It is stable for small k, while for large k, it becomes unstable and there appears a stable nontrivial equilibrium solution (Figure 3.3.1 (b)). The global structure of equilibrium solutions is shown in Figure 3.11, which clearly indicates the appearance of a supercritical pitchfork bifurcation when k is increased.

(II) Coupling of $(\tilde{u}^*(x), \tilde{v}^*(x))$ and $({}^*\tilde{u}(x), {}^*\tilde{v}(x))$

We still assume that τ is large, and consider the case $(u_1, v_1; u_2, v_2) = (\tilde{u}^*(x), \tilde{v}^*(x); {}^*\tilde{u}(x), {}^*\tilde{v}(x))$ which is no longer a equilibrium solution of (3.10),

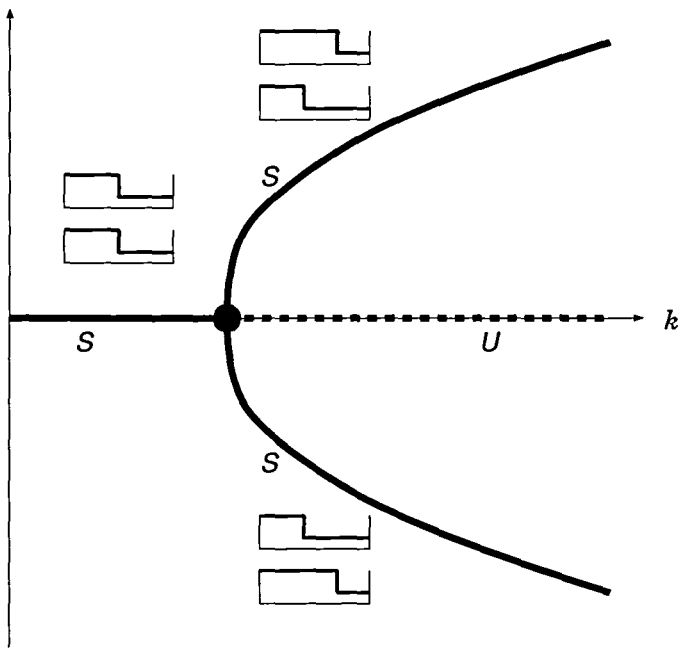

Figure 3.11: The global structure of the solution of the 1-layer coupled RD system for category (I). The solid line is the branch of the stable equlibrium solution, and the hashed line is that of the unstable one.

(3.11). Taking this function with or without small disturbances as the initial data, we find that the resulting solution tends to a unique equilibrium solution $(u_1(x), v_1(x); u_2(x), v_2(x))$ for which $(u_1(x), v_1(x))$ and $(u_2(x), v_2(x))$ have the reflection property at $x = 1/2$ (Figure 3.12). The global structure of the equilibrium solution is drawn in Figure 3.13. Our numerical simulation shows that the solution branch is always stable and there is no bifurcation phenomenon when k is varied.

(III) Coupling of periodic solutions bifurcating from $(\tilde{u}^*(x), \tilde{v}^*(x))$

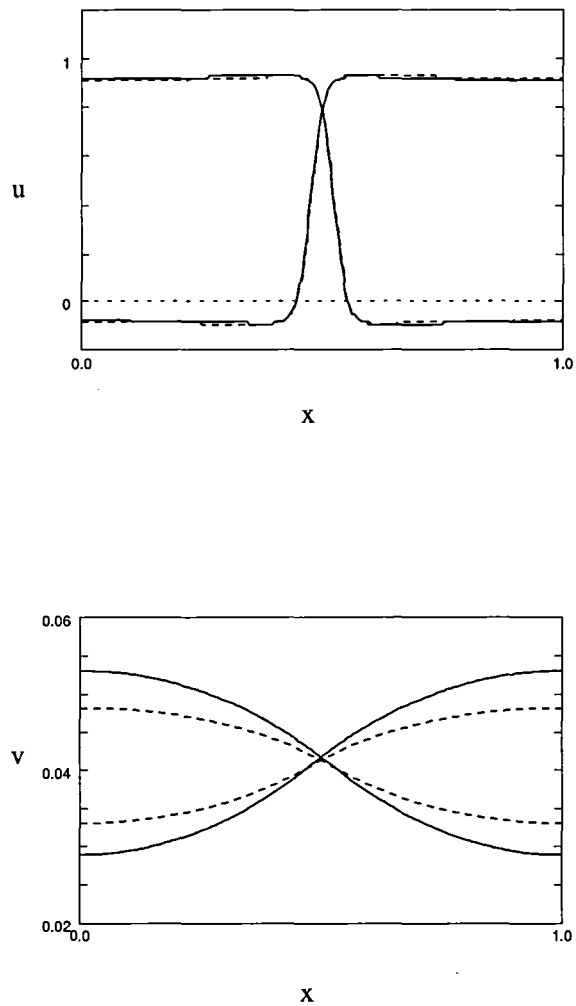

Figure 3.12: The spatial profiles of u_1, u_2 (top) and v_1, v_2 (bottom) of the unique equilibrium solution of the 1-layer coupled RD system, (3.8), (3.9), where $\tau = 0.2, \varepsilon = 0.01, d = 4, \alpha = 0.25, \gamma = 1, \theta = -0.4, L = 1$ in the case of $k = 5$ (solid lines) and $k = 20$ (hashed lines).

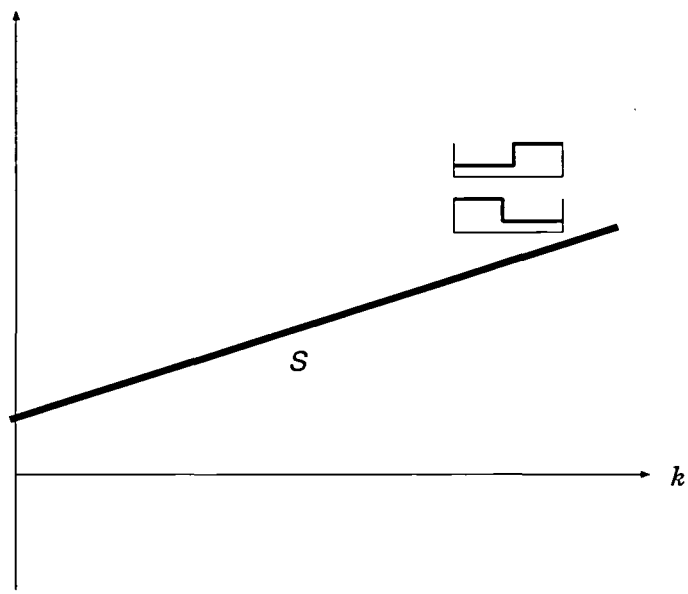

Figure 3.13: The global structure of the solution of the 1-layer coupled RD system for category (II).

and $(\tilde{u}^*(x), \tilde{v}^*(x))$

This case is similar to (I) except that $(\tilde{u}^*(x), \tilde{v}^*(x))$ is unstable in the decoupled system. Under this situation, there is a spatio-temporal periodic solution $(u^{*p}(x,t), v^{*p}(x,t))$ with an oscillating layer in the decoupled system (Figure 3.14). We study the coupling of this periodic solution in (3.8), (3.9). Taking $(u_1, v_1) = (u^{*p}(x,t), v^{*p}(x,t))$ and $(u_2, v_2) = (u^{*p}(x,t+s), v^{*p}(x,t+s))$ with small disturbances as initial data where $s(0 \leq s \leq T)$ is arbitrary phase difference within the period T, we numerically show that for small k, the solution tends to the trivial periodic solution $(u_1, v_1) = (u_2, v_2) = (u^{*p}(x,t+s_0), v^{*p}(x,t+s_0))$ for some $s_0(0 \leq s_0 \leq T)$; that is, the trivial

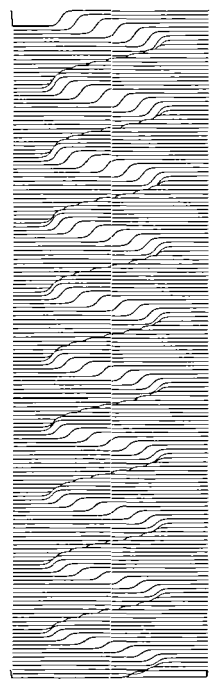

Figure 3.14: The dynamics of the oscillatory solution u of the 1-layer RD system, (3.10), (3.11), where $\tau = 0.08, \varepsilon = 0.01, d = 4, \alpha = 0.25, \gamma = 1, \theta = -0.4, L = 1$.

periodic solution is orbitally stable in the coupled system (Figure 3.15). On the other hand, for large k, oscillation of the solution is damped out, and then the solution tends to the nontrivial equilibrium solution which is the same as in the case (I) (Figure 3.16). The result indicates that the trivial periodic solution is destabilized and a nontrivial equilibrium solution is stabilized when k increases. More precisely speaking, there are two cases for the stability of equilibrium solutions depending on the value of τ; there is

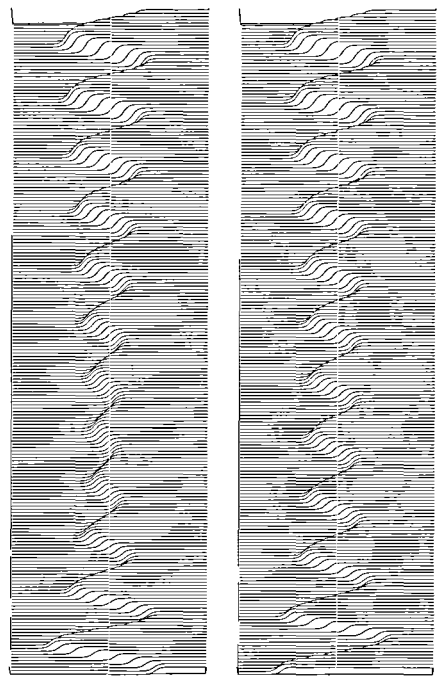

u_1 u_2

Figure 3.15: The dynamics of the 1-layer solution (u_1, u_2) for the coupled RD system, (3.8), (3.9), where $k = 1, \tau = 0.08, \varepsilon = 0.01, d = 4, \alpha = 0.25, \gamma = 1, \theta = -0.4, L = 1$. Two periodic solutions with different initial phase shift entrain to the trivial periodic solution.

the critical value $\tau^\sharp$ such that when $0 < \tau < \tau^\sharp$ two Hopf bifurcation points, say A and B, lie on the nontrivial equilibrium solution branch (Figure 3.17 (a)), and when $\tau^\sharp < \tau < \tau^*$, one Hopf bifurcation point, A', lies on the trivial equilibrium solution branch and the other, B', lies on the nontrivial equilibrium solution branch (Figure 3.17 (b)). The nontrivial equilibrium

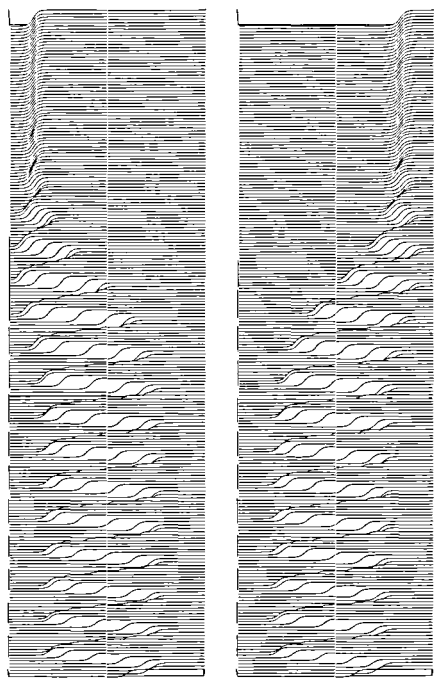

u_1 u_2

Figure 3.16: Trivial periodic solution tends to the stationary nontrivial equilibrium solution as in Figure 3.3.1, where $k = 25, \tau = 0.08, \varepsilon = 0.01, d = 4, \alpha = 0.25, \gamma = 1, \theta = -0.4, L = 1$.

solutions recover their stability when k passes the second Hopf bifurcation point, B (respectively B'). We note that the exchange of stability occurs between the trivial periodic solution and the nontrivial equilibrium one, which suggests the existence of the nontrivial periodic solution bifurcating from the nontrivial equilibrium solution branch at the point B (respectively B') which connects with the trivial periodic solution branch at C (respectively C').

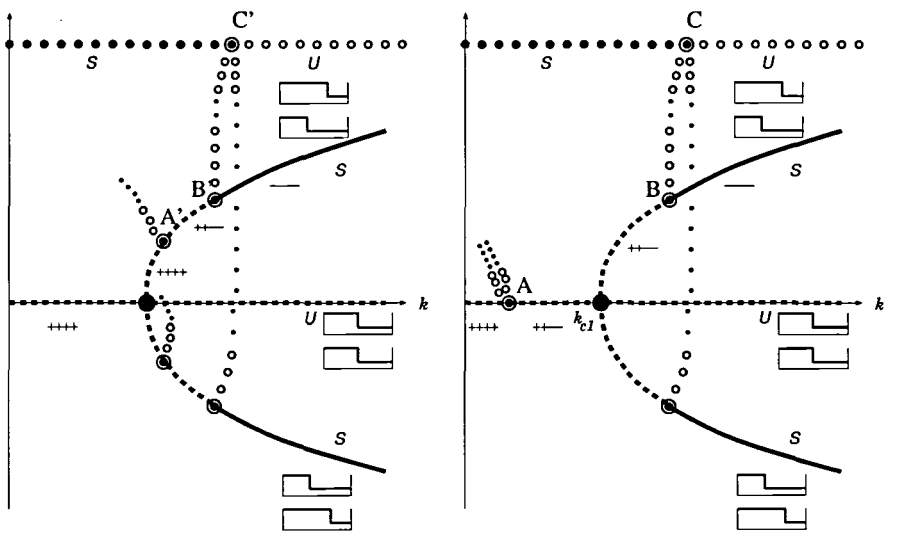

(a) (b)

Figure 3.17: The global structure of the solution of the 1-layer coupled RD system for category (III), where the solid lines describe the stable equilibrium solution, the hashed lines describe the unstable equlibrium branch, and the small circles describe trivial periodic solutions; the black circles are stable ones and the white circles are unstable ones. Furthermore double circles show the Hopf bifurcation points. (a) When $0 < \tau < \tau^\sharp$, 2 Hopf bifurcation points are located on the nontrivial equilibrium branch. (b) When $\tau^\sharp < \tau < \tau^*$, 2 Hopf bifurcation points exist so that one is located on the trivial equilibrium branch, and another is located on the nontrivial equilibrium branch.

Unfortunately, we have not yet been able to show the complete diagram for solutions bifurcating from A and A'.

(IV) Coupling of periodic solutions bifurcating from $(\tilde{u}^*(x), \tilde{v}^*(x))$ and $({}^*\tilde{u}(x), {}^*\tilde{v}(x))$

This situation is similar to the case (II), except that $(\tilde{u}^*(x), \tilde{v}^*(x))$ and $({}^*\tilde{u}(x), {}^*\tilde{v}(x))$ are unstable in the decoupled system under which there are periodic solutions $(u^{*p}(x,t), v^{*p}(x,t))$ and $({}^*u^p(x,t), {}^*v^p(x,t))$ with oscillating layers. This is also possible by taking the value of τ small as in case (III). We note that there uniquely exists the equilibrium solution which is shown in case (II). Taking these periodic functions with or without small disturbances as the initial data, we numerically solve the problem (3.8), (3.9). Then for small k, we find that the unique equilibrium solution is unstable and any solution tends to a unique periodic solution $(u_1(x,t), v_1(x,t); u_2(x,t), v_2(x,t))$ which satisfies $u_1(x,t) = u_2(1-x,t)$ and $v_1(x,t) = v_2(1-x,t)$ (Figure 3.18 (a)). On the other hand, for large k, the solution tends to the unique equilibrium solution (Figure 3.18 (b)). This indicates the recovery of stability of the equilibrium solution as k increases. It suggests that the stable periodic solution connects to the equilibrium solution branch at the Hopf bifurcation point B'' (Figure 3.19).

The above numerical results confirm that *no matter what the dynamics of the decoupled system is solutions of the coupled system generically tend to a nontrivial equilibrium solutions for large k.*

We will consider this problem for the case (I) and show that the trivial equilibrium solution becomes stable when k increases (Theorem 3.4.1) in Section 3.4.

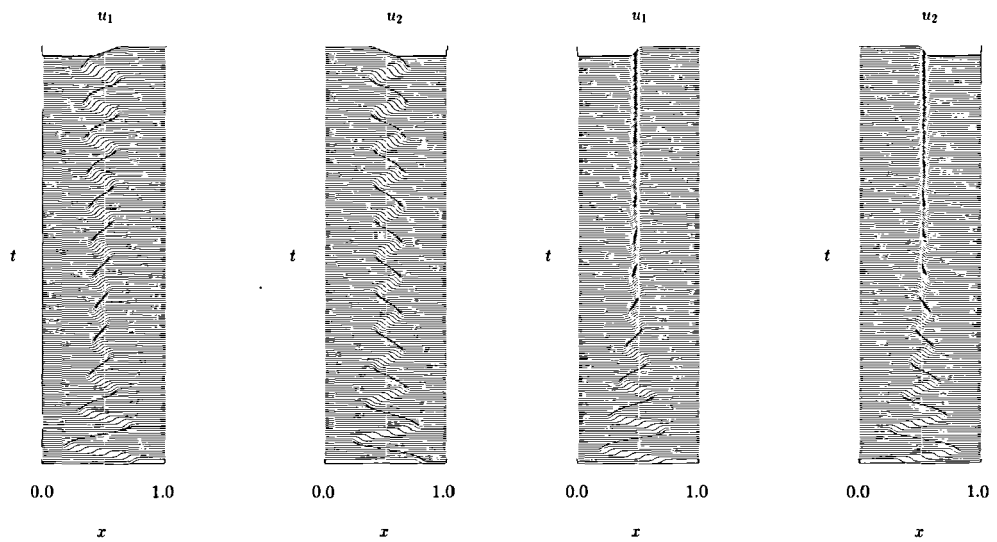

(a) (b)

Figure 3.18: The dynamics of the 1-layer solution u_1 and u_2 for the coupled RD system, (3.8), (3.9), where $\tau = 0.08, \varepsilon = 0.01, d = 4, \alpha = 0.25, \gamma = 1, \theta = -0.4, L = 1$. (a) When $k = 1$, two periodic solutions with different initial phase shift entrain to the unique nontrivial periodic solution. (b) When $k = 25$, periodic solution becomes stationary nontrivial solution which have the reflection property at $x = 1/2$ as in *Fiugre* 3.12.

3.3.2 2-layer case

In Section 3.3.1 we have found that for large τ there is a critical value k_{c1} such that when $0 < k < k_{c1}$, the trivial 1-layer equilibrium solution is stable, while, when $k > k_{c1}$, it becomes unstable, and nontrivial equilibrium solutions appear instead as a result of pitchfork bifurcation.

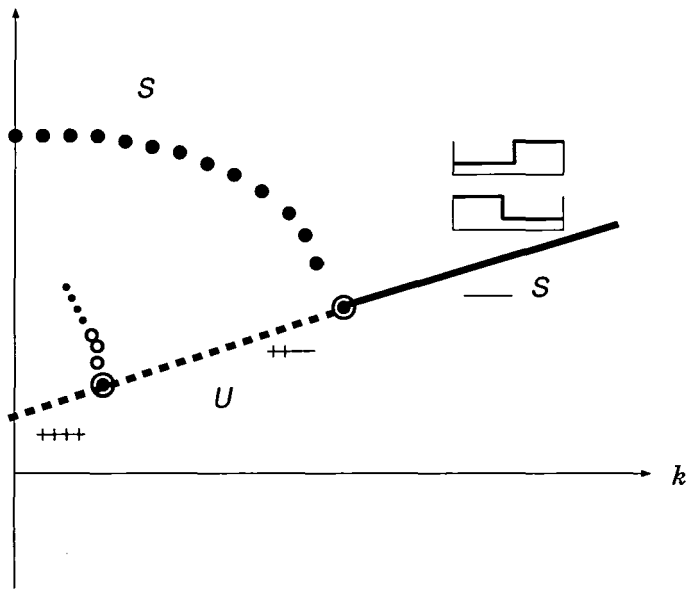

Figure 3.19: The global structure of the solution of the 1-layer coupled RD system for category (IV), where the solid lines describe the stable equilibrium solution, the hashed lines describe the unstable equilibrium solution, and the small circles describe the stable nontrivial periodic solutuion.

From the viewpoint of pattern formation, it is more interesting to study the coupling of multilayer equilibrium solutions. As the simplest case, we consider the coupling of 2-layer equilibrium solutions which are stable in the decoupled system. We take $L = 2$ so that two 2-layer equilibrium solutions can be directly constructed by reflecting of the 1-layer equilibrium solution symmetrically at $x = 1$ on the interval $(0, 2)$, as in Figure 3.20. Although there are two ways to do it as in Figure 3.20, we consider only the case of Figure 3.20 (a), because 3.20 (b) can be treated similarly. By the reflection

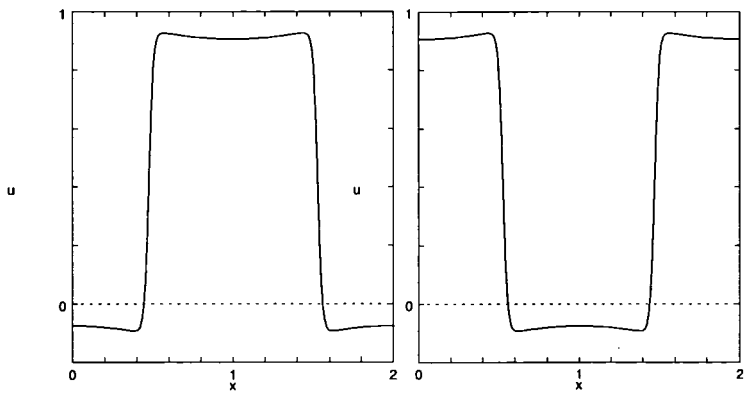

(a) (b)

Figure 3.20: The spatial profiles of u of the equilibrium solution of the 2-layer RD system, (3.10), (3.11), where $\tau = 0.2, \varepsilon = 0.01, d = 4, \alpha = 0.25, \gamma = 1, \theta = -0.4, L = 2$.

argument, it is clear from Figure 3.11 that there exists a global branch bifurcating from the trivial 2-layer equilibrium solution which is symmetric at $x = 1$. Recalling the result on the 1-layer equilibrium solutions, one would naturally like to ask the following two questions: "Is the trivial 2-layer equilibrium solution still stable for small k?" and "Is the nontrivial symmetric 2-layer equilibrium solution still stable for large k?"

In order to answer the questions, we fix τ to be large so that the 2-layer equilibrium solution is stable in the decoupled system. We first show the following result:

Proposition 3.3.1. *For a 2-layer equilibrium solution of the coupled system, there are two bifurcation points of pitchfork type when $k = k_{c1}$ and k_{c2} with*

$0 < k_{c2} < k_{c1}$, *such that the nontrivial symmetric and asymmetric equilibrium solutions bifurcate from the trivial equilibrium solution, at* $k = k_{c1}$ *and* $k = k_{c2}$, *respectively.*

The proof is found in Appendix C.

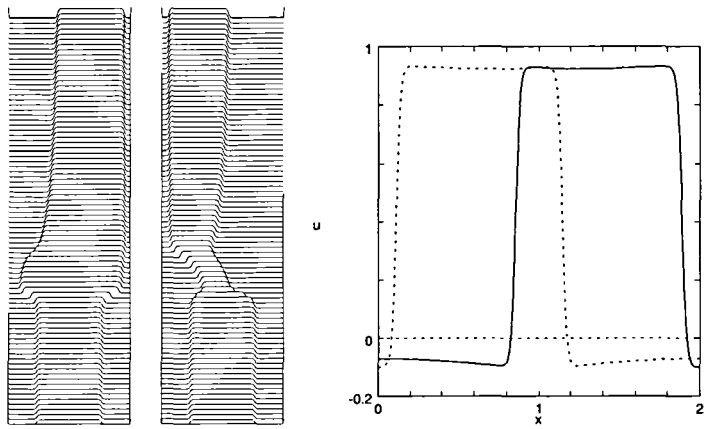

u_1 u_2

(a) (b)

Figure 3.21: (a) The dynamics of the 2-layer solution(u_1, u_2) for the coupled RD system, (3.8), (3.9), where $k = 20, \tau = 0.2, \varepsilon = 0.01, d = 4, \alpha = 0.25, \gamma = 1, \theta = -0.4, L = 2$. (b) The spatial profiles of u_1 (solid line) and u_2 (hashed line) of the nontrivial equilibrium solution.

Using this information on the bifurcation phenomena, we can numerically draw the global structure of equilibrium solutions with stability properties. (i) For $0 < k < k_{c2}$ the 2-layer trivial symmetric equilibrium solution is stable; and (ii) for $k_{c2} < k$ there is a stable 2-layer asymmetric equilibrium solution

of alternated pattern which is asymmetric with $x = 1$ as in Figure 3.21, and there are the nontrivial symmetric equilibrium solutions for $k_{c1} < k$, which are directly constructed by the reflection of the 1-layer solutions. What we emphasize here is the relation $k_{c2} < k_{c1}$; namely, asymmetric equilibrium solutions primarily bifurcate and symmetric ones do secondly from the trivial 2-layer solution when k increases. When k increases further, the primary branch remains stable and no secondary bifurcations on this branch occurs. The global picture of 2-layer equilibrium solutions is drawn in Figure 3.22.

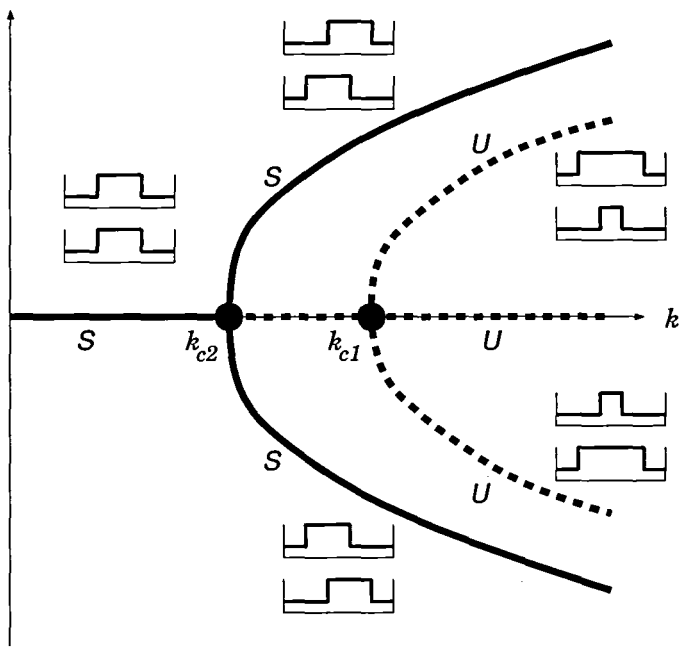

Figure 3.22: The global structure of the solution of the 2-layer coupled RD system where the trivial equilibrium solution is stable when $k = 0$.

3.3.3 Multilayer case

Let us continue to investigate the coupling of stable 4-layer equilibrium solutions. Taking $L = 4$, we find that such equilibrium solutions are easily constructed by flipping the 2-layer equilibrium solution at $x = 2$ in $(0, 4)$. Similar to the 2-layer case, it turns out that there is a critical value k_{c4} satisfying $0 < k_{c4} < k_{c2} < k_{c1}$ such that the trivial solution loses its stability at $k = k_{c4}$, and there appears instead a stable 4-layer asymmetric alternated pattern . On the other hand, by the reflection argument, the symmetric solutions also bifurcate at k_{c2} and k_{c1} from the trivial 4-layer branch; however these branches are unstable because the above alternated pattern already bifurcates primarily. The global picture of these solutions is drawn in Figure 3.23.

The observations indicate that for large τ the nontrivial equilibrium solutions of alternated type appear as a primary bifurcation from the trivial multilayer equilibrium solution, and there are no bifurcation on this nontrivial branch. This means that the nontrivial equilibrium solutions of alternated type are stable.

Next consider the case for small τ. In the situation similar to the category (III) of the 1-layer case, for small k the trivial periodic solution is stable, and there are no stable equilibrium patterns. However, when k increases, we numerically find that the exchange of stability occurs so that the trivial periodic solution loses its stability, and the equilibrium solutions of alternated type become stable. We thus arrive at the following plausible conjecture:

> An alternated pattern is stable for strong coupling (*i.e.*, large k) independently of the individual decoupled dynamics and the

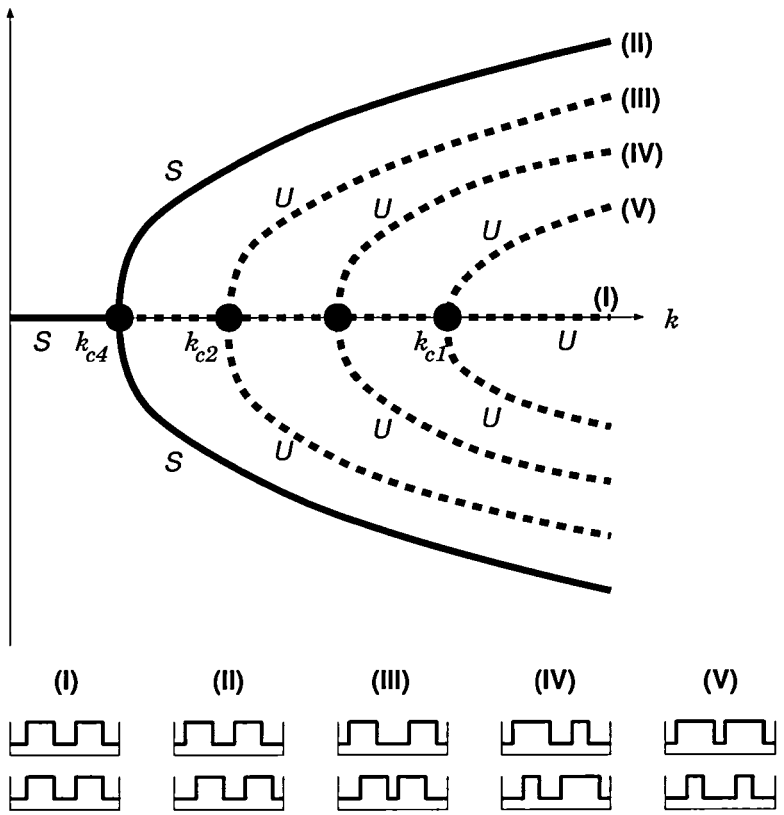

Figure 3.23: The global structure of the solution of the 4-layer solutions for the coupled RD system where the trivial equilibrium solution is stable when $k = 0$.

number of layers.

3.4 Stability analysis for 1-layer trivial equilibrium solution

By using the spectral analysis called the SLEP method, the decoupled system (*i.e.*, $k = 0$) was already studied in [24] when τ is employed as a bifurcation parameter.

As was seen in the Section 3.3.1 (I), increase of the coupling strength k causes destabilization of the trivial (or symmetric) solution, which is replaced by nontrivial (or asymmetric) ones. This is apparently a symmetry breaking bifurcation and could be detected by investigating the spectral behaviour with respect to k. If there are eigenvalues which cross the origin when k is varied, we call these *critical* real eigenvalues with k_c as the critical value of k.

The aim of this section is to give a rigorous proof to the bifurcation phenomenon with respect to k for the trivial 1-layer equilibrium solution when τ is fixed such that the equilibrium solution of the decoupled system is *stable*.

Let $(\tilde{u}(x;\varepsilon), \tilde{v}(x;\varepsilon))$ be the 1-layer equilibrium solution of (3.8) and (3.9). Substitute the following forms into (3.8),

$$\begin{cases} u_i(x,t) &= \tilde{u}(x;\varepsilon) + e^{\lambda t} w_i(x;\varepsilon) \\ v_i(x,t) &= \tilde{v}(x;\varepsilon) + e^{\lambda t} z_i(x;\varepsilon) \end{cases} \quad (i = 1, 2), \tag{3.21}$$

and use the symmetric and asymmetric expressions of w and z,

$$\begin{cases} w_s &= \frac{1}{2}(w_1 + w_2) \\ w_a &= \frac{1}{2}(w_1 - w_2) \\ z_s &= \frac{1}{2}(z_1 + z_2) \\ z_a &= \frac{1}{2}(z_1 - z_2). \end{cases} \tag{3.22}$$

Then, the resulting linearized eigenvalue problem of (3.8) is given by

$$\begin{cases} L^\varepsilon w_s + f_v^\varepsilon z_s &= \varepsilon\tau\lambda w_s \\ M^\varepsilon z_s + g_u^\varepsilon w_s &= \lambda z_s \\ L^\varepsilon w_a + f_v^\varepsilon z_a &= \varepsilon\tau\lambda w_a \\ (M^\varepsilon - 2k) z_a + g_u^\varepsilon w_a &= \lambda z_a \end{cases} \quad x \in I, \tag{3.23}$$

with $L^\varepsilon \equiv \varepsilon^2 \frac{d^2}{dx^2} + f_u^\varepsilon$ and $M^\varepsilon \equiv d\frac{d^2}{dx^2} + g_v^\varepsilon$, where $f_u^\varepsilon = f_u(\tilde{u}(x;\varepsilon), \tilde{v}(x;\varepsilon))$, $f_v^\varepsilon, g_u^\varepsilon$, and g_v^ε are similarly defined. The boundary conditions are

$$\begin{cases} \frac{\partial w_i}{\partial n} &= 0 \\ \frac{\partial z_i}{\partial n} &= 0 \end{cases} \quad (i = s, a), x \in \partial I. \tag{3.24}$$

In our setting, two RD systems have the same parameters, ε, τ, α, γ, θ, so that the symmetric and asymmetric parts, (w_s, z_s) and (w_a, z_a), are decoupled as in (3.23). Apparently the symmetric part, (w_s, z_s), is exactly the same as that of the decoupled RD system of the category (I) in Section

3.3.1, and hence it has only stable eigenvalues. Therefore we may investigate only the coupling effect for the second system of (3.23) for (w_a, z_a), including the coupling parameter k. In a parallel way to the one in [24], we can derive the following singular limit eigenvalue problem of (3.23) for the asymmetric part (w_a, z_a). The outline of the proof is as follows (for details, see Appendix A): For simplicity, we write (w_a, z_a) as (w, z) without confusion. First we rewrite (3.23) as the equation for z_R and z_I, which are real and imaginary parts of z, respectively, with the complete orthonormal set of eigenfunctions and eigenvalues $\{\phi_j^\varepsilon, \zeta_j^\varepsilon\}_{j=0}^\infty$ of the Sturm-Liouville operator for L^ε. Then, taking the singular limit as $\varepsilon \downarrow 0$, we derive the equations for z_R^* and z_I^*, where $z_R^* = \lim_{\varepsilon \downarrow 0} z_R$ and $z_I^* = \lim_{\varepsilon \downarrow 0} z_I$. We set the Dirac's δ-function at x^* as $\delta^* = \delta(x^*)$, where x^* is the limiting position of the internal transition layer of the decoupled 1-layer system (3.10), (3.11) as $\varepsilon \downarrow 0$. Letting $< \cdot, \cdot >$ be the $\mathbf{L}^2$-pairing and operating $< \cdot, \delta^* >$ to each side of these equations, we get the following equation:

$$N_k \begin{pmatrix} < z_R^*, \delta^* > \\ \\ < z_I^*, \delta^* > \end{pmatrix} = 0,$$

where N_k is the 2x2 matrix depending on the parameter k (the derivation is found in Appendix A). Consequently the necessary and sufficient condition for the existence of nontrivial solution of ${}^t(< z_R^*, \delta^* >, < z_I^*, \delta^* >)$ is given by

$$\begin{aligned} 0 &= det\ N_k \\ &= \{\frac{\hat{\Xi}_0^*}{\hat{\Delta}_0^*} A_k + \frac{\tau(\lambda_I^*)^2}{\hat{\Delta}_0^*} B_k - 1\}^2 + \{\frac{\tau \lambda_I^*}{\hat{\Delta}_0^*} A_k - \frac{\hat{\Xi}_0^* \lambda_I^*}{\hat{\Delta}_0^*} B_k\}^2, \end{aligned} \tag{3.25}$$

where $\lim_{\varepsilon\downarrow 0}\lambda = \lambda^* = \lambda_R^* + i\lambda_I^*$, $\hat{\Xi}_0^* = \hat{\zeta}_0^* - \tau\lambda_R^*$, and $\hat{\Delta}_0^* = (\hat{\zeta}_0^* - \tau\lambda_R^*)^2 + (\tau\lambda_I^*)^2$. It is already known in [24] $\lim_{\varepsilon\downarrow 0}(\zeta_0/\varepsilon) = \hat{\zeta}_0^* > 0$ where ζ_0 is the principal eigenvalue of the Sturm-Liouville operator L^ε. A_k and B_k are respectively defined by

$$\begin{cases} A_k &= < \hat{I}_{\lambda_R^*+2k} K_{\lambda_R^*+2k}(\hat{c}\delta^*), \delta^* > \\ B_k &= < \hat{I}_{\lambda_R^*+2k}\{K_{\lambda_R^*+2k}\}^2(\hat{c}\delta^*), \delta^* >, \end{cases} \tag{3.26}$$

where $K_{\lambda_R^*+2k} = \left[-d\frac{d^2}{dx^2} - \frac{det^*}{f_u^*} + \lambda_R^* + 2k\right]^{-1}$, $\hat{I}_{\lambda_R^*+2k} \equiv [I + (\lambda_I^* K_{\lambda_R^*+2k})^2]^{-1}$, and $\hat{c} = c_1^* c_2^*$ where

$$\begin{aligned} c_1^* &= -\kappa^* \frac{d}{dv} J(v^*) > 0 \\ c_2^* &= \kappa^* \{g(h_+(v^*), v^*) - g(h_-(v^*), v^*)\} > 0, \end{aligned}$$

with a positive constant κ^* , $h_\pm(v)$ is defined in the higher (or lower) level plateau region that satisfies $f(h_\pm(v), v) = 0$, $J(v) = \int_{h_-(v)}^{h_+(v)} f(s,v)ds$, I is the identity operator, and $det^* = f_u^* g_v^* - g_u^* f_v^*$, where $f_u^* = \lim_{\varepsilon\downarrow 0} f_u^\varepsilon$, f_v^*, g_u^*, and g_v^* are similarly defined.

For later use, it is convenient to introduce the following notation:

$$\begin{cases} A_k &= A(\lambda_R^* + 2k, (\lambda_I^*)^2) \\ B_k &= B(\lambda_R^* + 2k, (\lambda_I^*)^2). \end{cases} \tag{3.27}$$

Then it turns out that

$$\begin{cases} A(\lambda_R^*, (\lambda_I^*)^2) &= < \hat{I}_{\lambda_R^*} K_{\lambda_R^*}(\hat{c}\delta^*), \delta^* > \\ B(\lambda_R^*, (\lambda_I^*)^2) &= < \hat{I}_{\lambda_R^*}\{K_{\lambda_R^*}\}^2(\hat{c}\delta^*), \delta^* >, \end{cases}$$

where $\hat{I}_{\lambda_R^*} = [I + (\lambda_I^* K_{\lambda_R^*})^2]^{-1}$, and $K_{\lambda_R^*} = \left[-d\frac{d^2}{dx^2} - \frac{det^*}{f_u^*} + \lambda_R^*\right]^{-1}$.

The equation (3.25) for $\lambda^* = \lambda_R^* + i\lambda_I^*$ is much more tractable than the original one and leads us to the following result for the stability of the trivial equilibrium solution.

Theorem 3.4.1 (Behaviour of singular limit eigenvalues). *Fix τ arbitrarily satisfying*

$$B(0,0) \leq \tau. \tag{3.28}$$

Then there exists $k_c > 0$ such that a unique real critical eigenvalue of (3.25) crosses the origin at $k = k_c$ transversally from negative to positive on the real axis. All the remaining eigenvalues lie strictly on the left side of imaginary axis, namely, the trivial solution is stable in the singular limit sense for $0 \leq k < k_c$, while it is unstable when $k > k_c$.

Note that the above results can be extended to small positive ε.

Theorem 3.4.2 (Symmetry breaking pitchfork bifurcation). *There exists $k_c^\varepsilon > 0$ for any small $\varepsilon > 0$ such that (a) when k increases, there exists a uniquie simple critical eigenvalue $\lambda^\varepsilon(k)$ of (3.23) such that it crosses the origin transversally from negative to positive on real axis at $k = k_c^\varepsilon$ when $\varepsilon \downarrow 0$, $\lambda^\varepsilon(k)$ and k_c^ε converge to $\lambda^*(k)$ and k_c of Theorem 3.4.1, respectively. (b) a symmetry breaking pitchfork bifurcation occurs at $k = k_c^\varepsilon$ and non-symmetric solutions emanate from the trivial branch like Figure 3.11. (c) at $k = k_c^\varepsilon$, all the rest of spectra of (3.23) lie strictly on left side of the imaginary axis, namely the pitchfork bifurcation (b) is a primary one.*

Once Theorem 3.4.1 is proved, Theorem 3.4.2 can be proved in a similar way to that of Theorem 4.1 of [24]. Hence we focus on the proof of Theorem

3.4.1. A noteworthy thing for the coupled system is that only real eigenvalues cause the instability under (3.28). Namely we have

Lemma 3.4.1 (No critical complex eigenvalues). *If τ and k_c satisfy the condition (3.28), there are no complex eigenvalues that cross the imaginary axis.*

We prove this lemma in Appendix B.

Lemma 3.4.2 (Existence of a bifurcation point and its transversality). **(a)** *(existence) For real eigenvalues, (3.25) is equivalent to*

$$F(\lambda_R^*, k) = 0, \tag{3.29}$$

where

$$F(\lambda_R^*, k) \equiv \hat{\zeta}_0^* - \tau\lambda_R^* - A(\lambda_R^* + 2k, 0) \tag{3.30}$$

For fixed τ, there exists a unique $k_c > 0$ that satisfies

$$F(0, k_c) = 0, \tag{3.31}$$

namely, there is a zero eigenvalue at $k = k_c$ which is simple.

(b) *(transversality) When condition (3.28) is satisfied, there is a positive constant δ_1 such that for k satisfying $|k - k_c| < \delta_1$ and $F(\lambda_R^*, k) = 0$, there exists a unique C^1-function*

$$\lambda_R^* = \lambda_R^*(k), \tag{3.32}$$

and a real eigenvalue λ_R^* crosses the origin transversally at $k = k_c$.

Remark 3.4.1. *In a similar way to [24], we can prove the following relation:*

$$B(\lambda_R, 0) = - \left. \frac{\partial A}{\partial \lambda_R} \right|_{\lambda_I = 0} \tag{3.33}$$

Proof of lemma 3.4.2

First we prove that there uniquely exists k_c such that zero eigenvalue exists.

By putting

$$\begin{aligned} \tilde{F}(k) &\equiv F(0,k) \\ &= \hat{\zeta}_0^* - A(2k,0), \end{aligned} \tag{3.34}$$

it follows from the Theorem 2.2 of [24] that

$$\tilde{F}(0) = \hat{\zeta}_0^* - A(0,0) < 0. \tag{3.35}$$

On the other hand, it follows from the Lemma 3.3 of [24] that

$$\lim_{k \to \infty} \tilde{F}(k) = \hat{\zeta}_0^* - \lim_{\lambda_R \to \infty} A(\lambda_R, 0) = \hat{\zeta}_0^* > 0 \tag{3.36}$$

and

$$\begin{aligned} \frac{d}{dk}\tilde{F}(k) &= -\frac{d}{dk}A(2k,0) \\ &= -2 \left. \frac{\partial A}{\partial \lambda_R} \right|_{\lambda_R = 2k, \lambda_I = 0} > 0 \end{aligned} \tag{3.37}$$

Hence, there exists a unique $k_c (> 0)$ satisfying the equation (3.31)

Next we show that this critical eigenvalue crosses the origin transversally when k is varied. Here, applying the implicit function theorem to $F(\lambda_R^*, k) = 0$ at $\lambda_R^* = 0$, $k = k_c$, we can determin the sign of $d\lambda_R^*/dk$.

Since the Lemma 3.2 of [24] implies that $B(0,0) > B(2k_c,0)$ for $k_c > 0$, it turns out that

$$\begin{aligned} \left.\frac{\partial F}{\partial \lambda_R}\right|_{\lambda_R=0,k=k_c} &= -\tau - \left.\frac{\partial A}{\partial \lambda_R}\right|_{\lambda_R=2k_c,\lambda_I=0} \\ &= -\tau + B(2k_c,0) \\ &< -\tau + B(0,0) \qquad\qquad < 0. \end{aligned} \tag{3.38}$$

The implicit function theorem tells us that there exists a positive constant δ_1 such that the unique function $\lambda_R^* = \lambda_R^*(k)$ defined for $|k-k_c| < \delta_1$, $\lambda_R^*(k)$ is real-analytic and continuous with respect to k when (3.28) is satisfied.

Differentiating (3.29) with respect to k at $\lambda_R^* = 0$ and $k = k_c$, we have

$$\begin{aligned} 0 &= \left.\frac{dF}{dk}\right|_{\lambda_R=0,k=k_c} \\ &= \left.\frac{\partial F}{\partial k}\right|_{\lambda_R=0,k=k_c} + \left.\frac{d\lambda_R^*}{dk}\right|_{k=k_c} \left.\frac{\partial F}{\partial \lambda_R}\right|_{\lambda_R=0,k=k_c} \\ &= -2\left.\frac{\partial A}{\partial \lambda_R}\right|_{\lambda_R=2k_c,\lambda_I=0} - \left.\frac{d\lambda_R^*}{dk}\right|_{k=k_c} \left[\tau + \left.\frac{\partial A}{\partial \lambda_R}\right|_{\lambda_R=2k_c,\lambda_I=0}\right]. \end{aligned} \tag{3.39}$$

Then, we find

$$\left.\frac{d\lambda_R^*}{dk}\right|_{k=k_c} = -\frac{2A'}{\tau + A'}, \tag{3.40}$$

where

$$A' = \left.\frac{\partial A}{\partial \lambda_R}\right|_{\lambda_R=2k_c,\lambda_I=0}. \tag{3.41}$$

Since Lemmas 3.2 and 3.3 of [24] and the inequality (3.28) tell us that for

$k_c > 0$

$$\begin{cases} A' < 0 \\ \tau + A' = \tau - B(2k_c, 0) > \tau - B(0,0) \geq 0, \end{cases} \tag{3.42}$$

we have

$$\left.\frac{d\lambda_R^*}{dk}\right|_{k=k_c} > 0 \tag{3.43}$$

where $\lambda_R^*(k_c) = 0$.

Consequently, one finds that the critical eigenvalue crosses the origin transversally at $k = k_c$.

Proof of Theorem 3.4.1

It is apparent that

$$\lambda_R^* \begin{cases} < 0 \text{ for } k_c - \delta_1 < k < k_c \\ = 0 \text{ for } k = k_c \\ > 0 \text{ for } k_c < k < k_c + \delta_1. \end{cases} \tag{3.44}$$

The simplicity of this critical eigenvalue can be proved by using the same discussion as in Theorem 4.1 of [24], although the complex eigenvalue was treated there.

In view of Proposition 2.2 of [15] it is easily seen that the simple bifurcation at $k = k_c$ is of pitchfork type.

Although we do not discuss the direction of this bifurcation, our numerical results suggest that the pitchfork bifurcation occurs super-critically at $k = k_c$.

3.5 Concluding remarks

In the previous sections, we have investigated the stability of the trivial equilibrium solution of the coupled RD system (3.6) with (3.7), and have observed that the stationary patterns of alternated type become stable ones regardless to the dynamics property of the decoupled system when the coupling strength k becomes large. Let us state this more precisely for the case of 1-layer solutions. For large τ, the trivial 1-layer equilibrium solution remains stable for weak coupling (*i.e.* small k), while it loses stability at the critical value $k = k_c$, and the nontrivial equilibrium solutions of alternated type appear via symmetry breaking pitchfork bifurcation, which persist as stable solutions for strong coupling (*i.e.* large k). On the other hand, for small τ, the trivial equilibrium solution is already destabilized, and instead there appears a stable periodic solution with oscillating layers in the decoupled system. Under this situation, there are two critical points C (respectively C'), and B (respectively B') as in Figure 3.17, such that, increasing the value of k, the trivial periodic solution loses its stability as it passes C (respectively C') and the nontrivial equilibrium solutions of alternated type become stable as it passes B (respectively B').

The fact that alternated patterns dominate the dynamics for large k also explains the stability of the anti-phase coupling patterns (category (II) and (IV) of Section 3.3.1). It seems a common feature for 2 dimensional coupling patterns as is demonstarated in Figure 3.6.

Finally we make one remark that although we have restricted the kinetics to Turing type, the result holds true for the other cases such as bistable and excitable types. That is, the alternated stationary pattern develops

generically if the coupling is strong. This is an essential feature of coupled RD systems.

Chapter 4

Summary

In this thesis, the bifurcation structures of dynamics of two types of the reaction-diffusion systems are investigated.

In Chapter 2, crack evolution model is investigated. Generally speaking, it is hard to confirm the crack evolution phenomena repeatedly on both experiment and numerical simulation. Because many scheme is developed for resolving these difficulties, it is considered that special scheme for numerical simulation of the crack evolution problem is necessary. The PDE equations that is simple enough to solve the problem numerically is obtained from introducing the phase field for describing the cracked region (and also the damaged region). Using this models several numerical example of crack growth computed, and the bifurcation phenomena of the growth of two cracks is found. These equations require only the fixed domain for numerical simulation. It is realized to solve these phenomena using well-known numerical scheme such as finite difference method, finite volume method.

In Chapter 3, a simplified coupled reaction-diffusion system is derived

from a diffusive membrane coupling of two reaction-diffusion systems of activator-inhibitor type. It is shown that the dynamics of the original decoupled systems persists for weak coupling, while new coupled *stationary* patterns of *alternated* type emerge at a critical strength of coupling and become stable for strong coupling independently of the dynamics of the decoupled systems. The approach which is used in this thesis is singular perturbation techniques and complementarily numerical methods.

The bifurcation phenomena of the dynamics of the reaction-diffusion systems is took up here. Those are the temporal evolution of the phase field that describes the cracked, and the temporal evolution of the profile of the concentration of the chemicals on the coupled reaction-diffusion system. Those can be categorized as followings: i) bifurcation phenomena that is parameterized by the constants of the equations, such as time constants, diffusion constants, and energy constants, ii) bifurcation phenomena that is parameterized by the initial pattern, profile of the valiables. The crack evolution problem is categorized into ii), and the coupled reaction-diffusion system is categorized into i). In this thesis, the bifurcation phenomena is investigated by the results of the temporal evolution using numerical simulation. However, from the view point to analyze the bifurcation structure numerically on i), such as coupled reaction-diffusion system, it is also possible to use the branch-tracking approach, like AUTO. It is expected that the global bifurcation structure of the coupled reaction-diffusion system may be more clear using the results of the temporal evolution and the branch-tracking complementarily.

ACKNOWLEDGEMENT

My deepest appreciation goes to Prof. Nakaki who gave me invaluable comments and warm encouragements throughout the course of this thesis. I have great honor to acknowlege Prof. Mimura and Prof. Nishiura who introduced the reaction diffusion problem to me, and I learned the basics of spatio-temporal pattern formation from them. I am also deeply grateful to Prof. Kimura for introducing this crack evolution problem and making fruitful discussions on this. Special thanks also goes to Prof. Tomoeda and Prof. Ohtsuka, they showed interest on my study and provided a forum for presentation. I would also like to express my gratitude to my family for their moral support and warm encouragements.

Bibliography

[1] L. Ambrosio and V. M. Tortorelli, On the approximation of free discontinuity problems, Boll. Un. Mat. Ital. (7) 6-B, (1992) 105-123.

[2] B. Bourdin, *The variational formulation of brittle fracture: numerical implementation and extensions.* preprint (2006), to appear in IUTAM Symposium on Discretization Methods for Evolving Discontinuities (T. Belytschko, A. Combescure, and R. de Borst eds.), Springer.

[3] B. Bourdin, *Numerical implementation of the variational formulation of brittle fracture.* Interfaces Free Bound., Vol.9 (2007) 411-430.

[4] B. Bourdin, G. A. Francfort and J.-J. Marigo, *Numerical experiments in revisited brittle fracture.* J. Mech. Phys. Solids, Vol.48, No.4 (2000), 797-826.

[5] M. Buliga, *Energy minimizing brittle crack propagation.* J. Elasticity, Vol.52, No.3 (1998/99), 201-238.

[6] C. M. Elliott and J. R. Ockendon, *Weak and variational methods for moving boundary problems.* Pitman Publishing Inc. (1982)

[7] G. A. Francfort and J.-J. Marigo, *Revisiting brittle fracture as an energy minimization problem.* J. Mech. Phys. Solids, Vol.46 (1998), 1319-1342.

[8] A. A. Griffith, *The phenomenon of rupture and flow in solids.* Phil. Trans. Royal Soc. London, A221 (1920), 163-198.

[9] M. Hori, K. Oguni and H. Sakaguchi, Proposal of FEM implemented with particle discretization for analysis of failure phenomena, J. of the Mech. and Phys. of Sol., Vol.53 (2005), 681-703.

[10] M. Kimura, H. Komura, M. Mimura, H. Miyoshi, T. Takaishi, and D. Ueyama, Adaptive mesh finite element method for pattern dynamics in reaction-diffusion systems. in: Proc. of the Czech-Japanese Seminar in Applied Mathematics 2005, COE Lecture Note Vol.3, Faculty of Mathematics, Kyushu University ISSN 1881-4042(2006), 56-68.

[11] M. Kimura, H. Komura, M. Mimura, H. Miyoshi, T. Takaishi, and D. Ueyama, Quantitative study of adaptive mesh FEM with localization index of pattern, in: Proc. of the Czech-Japanese Seminar in Applied Mathematics 2006, COE Lecture Note Vol.6, Faculty of Mathematics, Kyushu University ISSN 1881-4042(2007), 114-136.

[12] R. Kobayashi, *Modeling and numerical simulations of dendritic crystal growth.* Physica D, Vol.63 (1993), 410-423.

[13] A. Schmidt and K. G. Siebert, *Design of Adaptive Finite Element Software. The Finite Element Toolbox ALBERTA*, Lecture Notes in Computational Science and Engineering, 42. Springer-Verlag, Berlin, 2005.

[14] A. Visintin, *Models of phase transitions.* Birkhauser (1996).

[15] H. Fujii, M. Mimura, and Y. Nishiura. *A picture of the global bifurcation diagram in ecologically interacting and diffusing systems.* Physica D, Vol.5, No.1 (1982), 1-42.

[16] A. Gierer and H. Meinhardt. *A theory of biological pattern formation.* Kybernetik, Vol.12 (1972) 30-39.

[17] P. De Kepper, V. Castets, E. Dulos, and J. Boissonade. *Turing-type chemical patterns in the chlorite-iodide-malonic acid reaction.* Physica D, Vol.49 (1991), 161-169.

[18] I. Lengyel and I. R. Epstein. *Modeling of turing structures in the chlorite-iodide-malonic acid-starch reaction sytem.* Science, Vol.251 (1991), 650-652.

[19] M. Mimura, M. Tabata, and Y. Hosono. *Multiple solutions of two-point boundary value problems of neumann type with a small parameter.* SIAM Journal of Mathematical Analysis, Vol.11 (1981), 613-631.

[20] J. D. Murray. *A pre-pattern formation mechanism for animal coat marking.* Journal of theoretical Biology, Vol.88 (1981), 161-199.

[21] J. D. Murray. *Mathematical Biology,* Springer-Verlag, 1989.

[22] Y. Nishiura. *Coexistence of infinitely many stable solutions to reaction diffusion systems in the singular limit.* Dynamics Reported (New series), Vol.3 (1994).

[23] Y. Nishiura and H. Fujii. *Stability of singular perturbed solutions to systems of reaction-diffusion equations.* SIAM J. Math. Anal., Vol.18, No.6 (1987), 1726-1770.

[24] Y. Nishiura and M. Mimura. *Layer oscillations in reaction-diffusion systems.* SIAM J. Appl. Math., Vol.49, No.2 (1989), 481-514.

[25] T. Ohta and H. Nakazawa. *Self-organization in an excitable reaction-diffusion system. ii. reduction to a coupled oscillator.* Physical Review A, Vol.45 (1992), 5504-5511.

[26] A. M. Turing. *The chemical basis of morphogenesis.* Phil. Trans. Royal Society London, Vol.B237 (1952), 37-72.

[27] A. T. Winfree. *The Geometry of Biological Time,* volume 8 of *Biomathematics.* Springer-Verlag, 1980.

[28] D. Winston, M. Arora, J. Maselko, V. Gáspár, and K. Showalter. *Cross-membrane coupling of chemical spatiotemporal patterns.* Nature, Vol.351 (1991), 132-135.

Appendix A

SLEP method for 1-layer coupled RD system

In this Appendix, we consider the eigenvalue problem of the coupled RD system for the trivial 1-layer equilibrium solution. First we make an assumption that the equilibrium solution of the decoupled system is stable.

We derive the eigenvalue equations from the linearized equations of (3.8), (3.9) around the 1-layer equilibrium solution $(\tilde{u}(x;\varepsilon),\tilde{v}(x;\varepsilon);\tilde{u}(x;\varepsilon),\tilde{v}(x;\varepsilon))$ and write it in symmetric and asymmetric components $(w_s(x;\varepsilon),z_s(x;\varepsilon))$ and $(w_a(x;\varepsilon),z_a(x;\varepsilon))$ as follows:

$$\begin{cases} L^\varepsilon w_s + f_v^\varepsilon z_s &= \varepsilon\tau\lambda w_s \\ M^\varepsilon z_s + g_u^\varepsilon w_s &= \lambda z_s \\ L^\varepsilon w_a + f_v^\varepsilon z_a &= \varepsilon\tau\lambda w_a \\ (M^\varepsilon - 2k) z_a + g_u^\varepsilon w_a &= \lambda z_a \end{cases} \qquad x \in I \tag{A.1}$$

with $L^\varepsilon \equiv \varepsilon^2 \dfrac{d^2}{dx^2} + f_u^\varepsilon$ and $M^\varepsilon \equiv d\dfrac{d^2}{dx^2} + g_v^\varepsilon$, where $f_u^\varepsilon = f_u(\tilde{u}(x;\varepsilon),\tilde{v}(x;\varepsilon))$, f_v^ε, g_u^ε, and

g_v^ε are similarly defined. The boundary conditions for (A.1) are

$$\begin{cases} \dfrac{\partial w_i}{\partial x} = 0 \\ \dfrac{\partial z_i}{\partial x} = 0 \end{cases} \quad (i = s, a), x \in \partial I \tag{A.2}$$

Obviously, one notices that the equations for (w_s, z_s) and (w_a, z_a), are completely separated, and the equations for (w_s, z_s) with (A.1), (A.2) are the eigenvalue problem of the decoupled system (3.10), (3.11). Therefore, we do not need to study the distribution of eigenvalues of this problem for (w_s, z_s) because of the assumption on the stability of the 1-layer equilibrium solution of the decoupled equilibrium solution. We thus only study the eigenvalue problem of asymmetric component (w_a, z_a), because it determines the stability of the trivial solution of the coupled system (3.8), (3.9). We may simply write (w_a, z_a) as (w, z) without confusion.

We consider the dependency of the distribution of eigenvalues of (A.1) when k is varied. To do this, we put $\lambda = \lambda_R + i\,\lambda_I$, $w = w_R + i\,w_I$, and $z = z_R + i\,z_I$, where λ_R and λ_I are real and imaginary parts of λ, respectively. Rewrite (A.1) as

$$\begin{cases} L^\varepsilon w_R + f_v^\varepsilon z_R = \varepsilon\tau(\lambda_R w_R - \lambda_I w_I) \\ L^\varepsilon w_I + f_v^\varepsilon z_I = \varepsilon\tau(\lambda_I w_R + \lambda_R w_I) \\ (M^\varepsilon - 2k) z_R + g_u^\varepsilon w_R = \lambda_R z_R - \lambda_I z_I \\ (M^\varepsilon - 2k) z_I + g_u^\varepsilon w_I = \lambda_I z_R + \lambda_R z_I. \end{cases} \tag{A.3}$$

Following the discussion similar to the one on the decoupled system in [24], we write (A.3) as

$$\begin{cases} w_R = [I + (\varepsilon\tau\lambda_I)^2 (L^\varepsilon - \varepsilon\tau\lambda_R)^{-2}]^{-1} \\ \qquad [(L^\varepsilon - \varepsilon\tau\lambda_R)^{-1}(-f_v^\varepsilon z_R) - \varepsilon\tau\lambda_I (L^\varepsilon - \varepsilon\tau\lambda_R)^{-2}(-f_v^\varepsilon z_I)] \\ w_I = [I + (\varepsilon\tau\lambda_I)^2 (L^\varepsilon - \varepsilon\tau\lambda_R)^{-2}]^{-1} \\ \qquad [(L^\varepsilon - \varepsilon\tau\lambda_R)^{-1}(-f_v^\varepsilon z_I) + \varepsilon\tau\lambda_I (L^\varepsilon - \varepsilon\tau\lambda_R)^{-2}(-f_v^\varepsilon z_R)] \end{cases} \tag{A.4}$$

where I denotes the identity operator.

Using the complete orthonormal set of eigenfunctions and eigenvalues $\{\phi_j^\varepsilon, \zeta_j^\varepsilon\}_{j=0}^\infty$ of the Sturm-Liouville operator L^ε, we can expand (A.4) as follows:

$$\left\{ \begin{array}{rcccl} w_R &=& \displaystyle\sum_{n=0}^{\infty} w_R^n \phi_n^\varepsilon &=& w_R^0 \phi_0^\varepsilon + w_R^\dagger \\ w_I &=& \displaystyle\sum_{n=0}^{\infty} w_I^n \phi_n^\varepsilon &=& w_I^0 \phi_0^\varepsilon + w_I^\dagger \end{array} \right. \tag{A.5}$$

where $w_R^n = (\Xi_n^\varepsilon/\Delta_n^\varepsilon) < -f_v^\varepsilon z_R, \phi_n^\varepsilon > -(\varepsilon\tau\lambda_I/\Delta_n^\varepsilon) < -f_v^\varepsilon z_I, \phi_n^\varepsilon >$, and $w_I^n = (\Xi_n^\varepsilon/\Delta_n^\varepsilon) < -f_v^\varepsilon z_I, \phi_n^\varepsilon > +(\varepsilon\tau\lambda_I/\Delta_n^\varepsilon) < -f_v^\varepsilon z_R, \phi_n^\varepsilon >$, and $\Xi_n^\varepsilon = \zeta_n^\varepsilon - \varepsilon\tau\lambda_R$, $\Delta_n^\varepsilon = (\zeta_n^\varepsilon - \varepsilon\tau\lambda_R)^2 + (\varepsilon\tau\lambda_I)^2$. The most dangerous parts of the above expressions are $w_R^0\phi_0^\varepsilon$ and $w_I^0\phi_0^\varepsilon$ because their denominators and the numerators tend to zero as $\varepsilon \downarrow 0$. We call these the *singular* parts. The other parts $w_R^\dagger$ and $w_I^\dagger$ consist of the components orthogonal to ϕ_0^ε. We call these the nonsingular parts which are represented as

$$\left\{ \begin{array}{rcl} w_R^\dagger &=& [I + (\varepsilon\tau\lambda_I)^2 (L^\varepsilon - \varepsilon\tau\lambda_R)^{-2}]^\dagger \\ & & [(L^\varepsilon - \varepsilon\tau\lambda_R)^\dagger (-f_v^\varepsilon z_R) - \varepsilon\tau\lambda_I (L^\varepsilon - \varepsilon\tau\lambda_R)^{2\dagger} (-f_v^\varepsilon z_I)] \\ w_I^\dagger &=& [I + (\varepsilon\tau\lambda_I)^2 (L^\varepsilon - \varepsilon\tau\lambda_R)^{-2}]^\dagger \\ & & [(L^\varepsilon - \varepsilon\tau\lambda_R)^\dagger (-f_v^\varepsilon z_I) + \varepsilon\tau\lambda_I (L^\varepsilon - \varepsilon\tau\lambda_R)^{2\dagger} (-f_v^\varepsilon z_R)]. \end{array} \right. \tag{A.6}$$

Then, the linearized equations for asymmetric components are given as follows:

$$\begin{pmatrix} T_k^\varepsilon & -\lambda_I + \varepsilon\tau\lambda_I S^\varepsilon \\ \lambda_I - \varepsilon\tau\lambda_I S^\varepsilon & T_k^\varepsilon \end{pmatrix} \begin{pmatrix} z_R \\ z_I \end{pmatrix} = \hat{M}^\varepsilon \begin{pmatrix} < z_R, -f_v^\varepsilon \dfrac{\phi_0^\varepsilon}{\sqrt{\varepsilon}} > \\ < z_I, -f_v^\varepsilon \dfrac{\phi_0^\varepsilon}{\sqrt{\varepsilon}} > \end{pmatrix} g_u^\varepsilon \frac{\phi_0^\varepsilon}{\sqrt{\varepsilon}} \tag{A.7}$$

where

$$\begin{aligned} T_\nu^\varepsilon &\equiv -d\frac{d^2}{dx^2} + g_v^\varepsilon + \lambda_R + 2\nu \\ & \quad -g_u^\varepsilon [I + (\varepsilon\tau\lambda_I)^2 (L^\varepsilon - \varepsilon\tau\lambda_R)^{-2}]^\dagger (L^\varepsilon - \varepsilon\tau\lambda_R)^\dagger (-f_v^\varepsilon \cdot) \\ S^\varepsilon &\equiv [I + (\varepsilon\tau\lambda_I)^2 (L^\varepsilon - \varepsilon\tau\lambda_R)^{-2}]^\dagger (L^\varepsilon - \varepsilon\tau\lambda_R)^\dagger (-f_v^\varepsilon \cdot) \end{aligned}$$

and

$$\hat{M}^\varepsilon \equiv \begin{pmatrix} \frac{\hat{\Xi}_0^\varepsilon}{\hat{\Delta}_0^\varepsilon} & -\frac{\tau\lambda_I}{\hat{\Delta}_0^\varepsilon} \\ \frac{\tau\lambda_I}{\hat{\Delta}_0^\varepsilon} & \frac{\hat{\Xi}_0^\varepsilon}{\hat{\Delta}_0^\varepsilon} \end{pmatrix},$$

where $\hat{\Xi}_0^\varepsilon = \hat{\zeta}_0^\varepsilon - \tau\lambda_R$, $\hat{\Delta}_0^\varepsilon = (\hat{\zeta}_0^\varepsilon - \tau\lambda_R)^2 + (\tau\lambda_I)^2$, and $\hat{\zeta}_0^\varepsilon = \zeta_0^\varepsilon/\varepsilon$.

Now, taking the limit $\varepsilon \downarrow 0$, we get

$$\begin{cases} \lim_{\varepsilon\downarrow 0} \frac{-f_v^\varepsilon \phi_0^\varepsilon}{\sqrt{\varepsilon}} &= c_1^* \delta^* \\ \lim_{\varepsilon\downarrow 0} \frac{g_u^\varepsilon \phi_0^\varepsilon}{\sqrt{\varepsilon}} &= c_2^* \delta^* \end{cases}$$

where $\delta^* = \delta(x^*)$ with x^* being the position of the internal layer of the trivial 1-layer equilibrium solution (1.8) for singular limit $\varepsilon \downarrow 0$, and

$$\begin{aligned} c_1^* &= -\kappa^* \frac{d}{dv} J(v^*) > 0, \\ c_2^* &= \kappa^* \{ g(h_+(v^*), v^*) - g(h_-(v^*), v^*) \} > 0 \end{aligned}$$

where κ^* is a positive constant, $h_\pm(v)$ are defined as the left and right branches of $f(h_\pm(v), v) = 0$, respectively (see Figure 3.2), and $J(v) = \int_{h_-(v)}^{h_+(v)} f(s,v)ds$. In this limit, (A.7) becomes

$$\begin{pmatrix} T_{\lambda_R^*+2k} & -\lambda_I^* \\ \lambda_I * & T_{\lambda_R^*+2k} \end{pmatrix} \begin{pmatrix} z_R^* \\ z_I^* \end{pmatrix} = \hat{M}^* \begin{pmatrix} < z_R^*, \delta^* > \\ < z_I^*, \delta^* > \end{pmatrix} \hat{c}\delta^* \qquad \text{(A.8)}$$

where

$$T_{\lambda_R{}^*+2k} \equiv -d\frac{d^2}{dx^2} - \frac{det^*}{f_u^*} + \lambda_R{}^* + 2k$$

$$\lim_{\varepsilon\downarrow 0} \hat{M}^\varepsilon = \hat{M}^* \equiv \begin{pmatrix} \frac{\hat{\Xi}_0^*}{\hat{\Delta}_0^*} & -\frac{\tau\lambda_I^*}{\hat{\Delta}_0^*} \\ \frac{\tau\lambda_I^*}{\hat{\Delta}_0^*} & \frac{\hat{\Xi}_0^*}{\hat{\Delta}_0^*} \end{pmatrix}$$

and $\lim_{\varepsilon\downarrow 0}\lambda = \lambda_R^* + i\lambda_I^*$, $\lim_{\varepsilon\downarrow 0}\hat{\zeta}_0^\varepsilon = \hat{\zeta}_0^*$, $\hat{\Xi}_0^* = \hat{\zeta}_0^* - \tau\lambda_R^*$, $\hat{\Delta}_0^* = (\hat{\zeta}_0^* - \tau\lambda_R^*)^2 + (\tau\lambda_I^*)^2$, $det^* = f_u^* g_v^* - g_u^* f_v^*$, and $\hat{c} = c_1^* c_2^*$. From Lemma 2.4 of [24], it follows that

$$\exists K_{\lambda_R^*+2k} \equiv T_{\lambda_R^*+2k}^{-1} \quad \text{for} \quad \lambda_R^* + 2k > -\mu_1,$$

where μ_1 is a positive constant so that all the remaining eigenvalues are located in the half plane left to $Re(\lambda) = -\mu_1$ in λ-plane. Then, we can derive the equations for z_R^* and z_I^* as

$$\begin{pmatrix} z_R^* \\ z_I^* \end{pmatrix} = \hat{I}_{\lambda_R^*+2k} \begin{pmatrix} I & \lambda_I^* K_{\lambda_R^*+2k} \\ -\lambda_I^* K_{\lambda_R^*+2k} & I \end{pmatrix} \hat{M}^* \begin{pmatrix} < z_R^*, \delta^* > \\ < z_I^*, \delta^* > \end{pmatrix} K_{\lambda_R^*+2k}(\hat{c}\delta^*) \tag{A.9}$$

$$\hat{I}_{\lambda_R^*+2k} \equiv [I + (\lambda_I^* K_{\lambda_R^*+2k})^2]^{-1}.$$

Operating $< \cdot, \delta^* >$ to each side of (A.9), we have

$$N_k \begin{pmatrix} < z_R^*, \delta^* > \\ < z_I^*, \delta^* > \end{pmatrix} = 0 \tag{A.10}$$

where

$$N_k \equiv < \hat{I}_{\lambda_R^*+2k} \begin{pmatrix} I & {\lambda_I}^* K_{\lambda_R^*+2k} \\ -{\lambda_I}^* K_{\lambda_R^*+2k} & I \end{pmatrix} M^* K_{\lambda_R^*+2k}(\hat{c}\delta^*), \delta^* > -I.$$

Then, it turns out that

$$det\ N_k = 0 \tag{A.11}$$

is the necessary and sufficient condition to assure the existence of of nontrivial solutions of ${}^t(< z_R^*, \delta^* >, < z_I^*, \delta^* >)$. (A.11) can be rewritten as

$$\begin{aligned} 0 &= det\ N_k \\ &= \{\frac{\hat{\Xi}_0^*}{\hat{\Delta}_0^*} A_k + \frac{\tau(\lambda_I^*)^2}{\hat{\Delta}_0^*} B_k - 1\}^2 + \{\frac{\tau\lambda_I^*}{\hat{\Delta}_0^*} A_k - \frac{\hat{\Xi}_0^* \lambda_I^*}{\hat{\Delta}_0^*} B_k\}^2, \end{aligned} \tag{A.12}$$

where $A_k = < \hat{I}_{\lambda_R^*+2k} K_{\lambda_R^*+2k}(\hat{c}\delta^*), \delta^* >$ and $B_k = < \hat{I}_{\lambda_R^*+2k} \{K_{\lambda_R^*+2k}\}^2(\hat{c}\delta^*), \delta^* >$.

Then, (A.11) is equivalent to

$$\frac{\hat{\Xi}_0^*}{\hat{\Delta}_0^*} A_k + \frac{\tau(\lambda_I^*)^2}{\hat{\Delta}_0^*} B_k - 1 = 0 \tag{A.13}$$

and

$$\frac{\tau\lambda_I^*}{\hat{\Delta}_0^*} A_k - \frac{\hat{\Xi}_0^* \lambda_I^*}{\hat{\Delta}_0^*} B_k = 0. \tag{A.14}$$

Appendix B

Proof of Lemma 4.1

Now we assume that $\lambda_I^* \neq 0$ when τ satisfies equation (3.28). Then, we can eliminate A_k from (A.13), (A.14) and thus obtain

$$[(\hat{\zeta}_0^* - \tau\lambda_R^*)^2 + (\tau\lambda_I^*)^2](B_k - \tau) \;=\; 0. \tag{B.1}$$

From the condition (3.28), there exists $k > 0$ such that $|\lambda_R^*(k)| < \delta_0$ holds for $0 < \delta_0 < \mu_1$, which is of our concern such that $B_k < \tau$. $K_{\lambda_R^*}$ is a well-defined uniformly bounded operator from $H^{-1}(I)$ to $H_N^1(I)$ for $\lambda_R^* > -\mu_1$. Because

$$\begin{cases} \dfrac{\partial B_k}{\partial \lambda_R^*} \;<\; 0 \quad \text{for} \quad \lambda_R^* + 2k > 0 \\ \dfrac{\partial B_k}{\partial (\lambda_I^*)^2} \;<\; 0 \quad \text{for} \quad (\lambda_I^*)^2 \geq 0. \end{cases} \tag{B.2}$$

Then equation (3.25) cannot be satisfied.

Appendix C

Analysis of the primary bifurcation point for the 2-layer equilibrium solution

Applying the same change of variables as (3.22) to the linearized eigenvalue problem at 2-layer equilibrium solution, we obtain

$$\begin{cases} L^\varepsilon w_s + f_v^\varepsilon z_s &= \varepsilon\tau\lambda w_s \\ M^\varepsilon z_s + g_u^\varepsilon w_s &= \lambda z_s \\ L^\varepsilon w_a + f_v^\varepsilon z_a &= \varepsilon\tau\lambda w_a \\ (M^\varepsilon - 2k) z_a + g_u^\varepsilon w_a &= \lambda z_a \end{cases} \qquad x \in I = (0,2) \tag{C.1}$$

subject to the Neumann boundary conditions on ∂I. The first two equations of (C.1) for (w_s, z_s) are independent of k, and hence, from our assumption that the trivial 2-layer solution is stable, we see that they do not contribute to the critical eigenvalues.

The remaining two equations for (w_a, z_a),

$$\begin{cases} L^\varepsilon w_a + f_v^\varepsilon z_a &= \varepsilon\tau\lambda w_a \\ (M^\varepsilon - 2k) z_a + g_u^\varepsilon w_a &= \lambda z_a, \end{cases} \quad x \in I = (0,2) \tag{C.2}$$

has exactly the same form as (3.12) in [22] except for the k-dependency being replaced $\varepsilon\tau\lambda$ by λ.

The same arguments in [22] (see also [24]) holds for (C.2), in particular, it has two critical eigenvalues which can be obtained by solving the following two eigenvalues on the half interval with different boundary conditions:

$$\begin{cases} L^\varepsilon w_a + f_v^\varepsilon z_a &= \varepsilon\tau\lambda w_a \\ (M^\varepsilon - 2k) z_a + g_u^\varepsilon w_a &= \lambda z_a \\ (w_a)_x(0) &= 0 = (z_a)_x(0) \\ (w_a)_x(1) &= 0 = (z_a)_x(1) \end{cases} \quad x \in (0,1) \tag{C.3}$$

$$\begin{cases} L^\varepsilon w_a + f_v^\varepsilon z_a &= \varepsilon\tau\lambda w_a \\ (M^\varepsilon - 2k) z_a + g_u^\varepsilon w_a &= \lambda z_a \\ (w_a)_x(0) &= 0 = (z_a)_x(0) \\ w_a(1) &= 0 = z_a(1) \end{cases} \quad x \in (0,1) \tag{C.4}$$

It is apparent that the even (respectively odd) extention of (C.3) (respectively (C.4)) to $(0,2)$ becomes a solution of (C.2). Hence, the zero eigenvalue of (C.3) (respectively (C.4)) gives us a symmetric (respectively asymmetric) bifurcation point, respectively. What we have to do is to find k-values of (C.3) (or (C.4)) with $\lambda = 0$. The singular limit procedures as in [23] and [22] can be done in a similar way for (C.3) and (C.4), and the resulting singular limit problem is to find k satisfying

$$\left(d\frac{d^2}{dx^2} + \frac{det^*}{f_u^*} - 2k \right) z_a^* = -c^*\delta^*/\hat{\zeta}_0^*$$

subject to

$$(z_a^*)_x(0) = 0, \quad (z_a^*)_x(x^*) = 1$$

$$(z_a^*)_x(1)(\text{respectively } z_a^*(1)) = 0,$$

respectively.

Noting that $\hat{\zeta}^*$ does not depend on the boundary condition, we see that there exists a unique positive $k = k_{NN}$ (respectively k_{ND}) with $0 < k_{ND} < k_{NN}$. This proves Proposition 3.3.1, since $k_{c2} = k_{ND}$ and $k_{c1} = k_{NN}$.

公表論文

(1) Phase Field Model for Mode III Crack Growth in Two Dimensional Elasticity
T.Takaishi and M.Kimura
Kybernetika 45(4) (2009), 605-614.

(2) Pattern Formation in Coupled Reaction-Diffusion System
T.Takaishi, M.Mimura and Y.Nishiura
Japan Journal of Industrial and Applied Mathematics 12(3) (1995) 385-424.